Soil Biology and Biochemistry 197 (2024) 109536

Contents lists available at ScienceDirect

Soil Biology and Biochemistry

journal homepage: www.elsevier.com/locate/soilbio

Soil pore network effects on the fate of nitrous oxide as influenced by soil compaction, depth and water potential

Mansonia Pulido-Moncada [a,b,*], Søren O. Petersen [b], Timothy J. Clough [c], Lars J. Munkholm [b], Andrea Squartini [a], Matteo Longo [a], Nicola Dal Ferro [a], Francesco Morari [a]

[a] Department of Agronomy, Food, Natural Resources, Animals and Environment, University of Padua, Legnaro, PD, Italy
[b] Department of Agroecology, Aarhus University, Tjele, Denmark
[c] Department of Soil and Physical Sciences, Lincoln University, Lincoln, New Zealand

ARTICLE INFO

Keywords:
N_2O diffusion
Subsoil
X-ray CT
Connected pores

ABSTRACT

Soil physical properties may determine the fate of nitrous oxide (N_2O) in soil, but little is known about how soil compaction affects specific properties and their interactions. This study aimed to assess the impact of compaction on the soil pore functionality and architecture, and the effects on N_2O diffusion. Intact soil cores were sampled from lysimeters previously subjected to induced topsoil or subsoil compaction, as well as from uncompacted lysimeters. The soil cores were drained, sequentially, to −30, −50, and −100 h Pa to examine gas phase characteristics, each time followed by N_2O diffusion measurements after injecting N_2O at the bottom of the soil cores to simulate hotspots. Pore architecture was determined with X-ray microtomography. Results showed that soil compaction decreased pore volume, gas flow (convection and diffusion), and pore connectivity, and increased water-filled pore space, isolated pore ratios, and solid-to-pore distance, with a concomitant effect on N_2O diffusion. Changes in soil matric water potential did not influence the N_2O diffusion ratio (N_2O in the headspace/N_2O injected into the reservoir). The algorithmic evaluation of interacting effects revealed that pore connectivity was the best predictor for N_2O diffusion. In hierarchical order, the N_2O diffusion ratio could be explained by air permeability, pore connectivity and relative gas diffusivity. Multivariate analysis of functional and architectural pore characteristic parameters provided a comprehensive selection of factors driving N_2O diffusion within the soil layers. This is essential to understand the contribution of N_2O produced in agricultural soil to atmospheric emissions under climate change scenarios.

1. Introduction

The atmospheric concentration of nitrous oxide (N_2O), a long-lived greenhouse gas and ozone-depleting substance, has continued to increase over the last four decades (Tian et al., 2020). Agricultural soils are recognised as a major source of anthropogenic N_2O emissions (Chataut et al., 2023; Jones et al., 2023), but the microbial production and emission of N_2O are regulated by a range of hydrological factors, soil parameters, and their complex interactions (Bremner, 1997; Wang et al., 2021). Understanding these environmental controls can support the development of strategies for mitigation.

The primary source of N_2O emissions is the topsoil receiving fertilisers and organic inputs, but deeper soil layers, often overlooked, can also contribute to N_2O production and emissions (Clough et al., 2005). Subsoil N_2O production may be driven by factors such as the formation of reactive zones resulting from downward nitrate and organic carbon transport (Wolf et al., 2022), and unfavourable soil physical conditions such as compaction (Yang et al., 2022). Moreover, N_2O produced in the subsoil is not necessarily linearly related to N_2O released into the atmosphere (Clough et al., 2006; Wolf et al., 2022).

The contribution of subsoil N_2O production to surface fluxes has been highlighted as a hidden threat, which is relatively more important in annual cropping systems, and during dry periods where the topsoil is at a moisture content that limits N_2O production (Shcherbak and Robertson, 2019). Subsoil N_2O production can impact surface emissions by upward diffusion along a concentration gradient in response to drought periods and rewetting of the soil profile as reported for forest soils (Goldberg and Gebauer, 2009a, 2009b). The fate of N_2O produced in different soil layers will depend on the functional pathways for soil gas diffusion. The N_2O molecule may reach the atmosphere if the soil

* Corresponding author. Department of Agroecology, Aarhus University, Tjele, Denmark.
E-mail address: mansonia.pm@agro.au.dk (M. Pulido-Moncada).

https://doi.org/10.1016/j.soilbio.2024.109536
Received 12 February 2024; Received in revised form 14 July 2024; Accepted 15 July 2024
Available online 18 July 2024

structure and associated soil water content facilitate gas exchange (Balaine et al., 2013). If N_2O cannot readily diffuse to the soil surface it may be reduced to environmentally benign dinitrogen gas (N_2) either near the site of production or during transport through the soil profile. Microbes containing the N_2O reductase gene (*nosZ*) transform N_2O to N_2 (Hallin et al., 2018). It is well recognised that microbial biomass decreases with increasing soil depth and the potential for transformation of N_2O to N_2 may be lower in subsoils. Nitrous oxide reduction potential increases with residence time, which in turn is influenced by soil tortuosity (Laudone et al., 2011) and water content. Nitrous oxide may also be entrapped in air-filled pores but later released to the atmosphere following an increase in gas diffusivity when soil moisture decreases and improves pore connectivity (Clough et al., 2005; Rabot et al., 2015). Nitrous oxide in the subsoil may also be transported to groundwater and eventually released into the atmosphere (Shcherbak and Robertson, 2019).

The interacting effects of soil structure and soil moisture on the fate of N_2O throughout the soil profile make estimating the fate of N_2O challenging. Understanding how these interactions are affected by soil compaction-induced changes in pore network may provide insights into the dynamic anaerobic-aerobic processes that regulate N_2O production in soil (Chamindu Deepagoda et al., 2019a).

Soil compaction, by altering soil pore size distribution, influences the size and distribution of physical hotspots (poor soil structure) for N_2O production (Ball, 2013). Within these pore structure-related hotspots, under oxygen-limited conditions, it is expected that denitrification, a microbial pathway for N_2O production, will increase (Kravchenko et al., 2018; Rohe et al., 2021). Previous studies have shown increased N_2O emissions to be linked to compacted soils: such soils have reduced pore space, higher water-filled pore space (WFPS) (Bussell et al., 2021) and reduced relative gas diffusivity (D_s/D_o) (Chamindu Deepagoda et al., 2019a). If such conditions are prolonged then anaerobic conditions may prevail, and N_2O is potentially reduced to N_2 (Chamindu Deepagoda et al., 2019b). Therefore, the occurrence and intensity of N_2O emissions from compacted soil layers may vary dynamically with soil structural conditions (pore size distribution, pore tortuosity, connectivity) and microbial substrate availability (Rabot et al., 2015).

Several studies have assessed the impact of soil compaction on N_2O fluxes, but often considering only how this affects the association between N_2O fluxes and WFPS, while other studies have observed gas diffusivity as the main controlling variable as summarised by Pulido-Moncada et al. (2022). However, interpreting the contribution of soil structural changes to N_2O fluxes as a result of changes in WFPS and gas diffusivity alone is difficult due to complex interacting factors and the simultaneous occurrence of denitrification. Such relationships are, initially, best examined in controlled incubation experiments.

Studies assessing the fate of N_2O within soil layers, and especially subsoil layers, where they considered multiple factors and processes, are limited. Examples of comprehensive incubation experiments using repacked soil columns to study drivers of the fate of N_2O within soil include those by Clough et al. (2006), Klefoth et al. (2014), Dong et al. (2020b), Hung and Whalen (2020), Roscioli et al. (2021), and Gil-Loaiza et al. (2022), where individual or combinations of factors such as relative gas diffusivity, soil microbiome, soil moisture content, biochar amendment, soil temperature (thawing of frozen soil), bulk density and dry/wet cycles were assessed. The study by Button et al. (2023) is an example using intact soil cores taken from topsoil and subsoil, and Goldberg and Gebauer (2009a, 2009b) are examples of field experiments.

However, to enhance our understanding of the fate of N_2O within individual soil layers, it is critically important to also consider the detailed soil structure status, such as variations in the morphology of the pore network (Rabot et al., 2015). Studies using X-ray micro-computed tomography (μCT) have suggested that the description of N_2O production and subsequent emissions could be improved by image-derived parameters such as the size and connectivity of air-filled pore networks (Rabot et al., 2015; Schlüter et al., 2019; Kim et al., 2022), the anaerobic soil volume fraction (Kravchenko et al., 2018; Rohe et al., 2021), and by the volume and spatial distribution of hotspots created by particulate organic matter and their proximity to air-filled pores (Kravchenko et al., 2018; Lucas et al., 2023; Ortega-Ramírez et al., 2023). Despite a large body of research on N_2O production and transport in agricultural soils, the effects of changes in soil pore network characteristics on N_2O fluxes from soils with different degrees of compaction are poorly understood and documented, as highlighted by Pulido-Moncada et al. (2022).

Thus, knowledge gaps remain about how soil compaction affects soil structural properties and their interactions with respect to the fate of N_2O within soil layers (Hernandez-Ramirez et al., 2021; Hu et al., 2021; Pulido-Moncada et al., 2022). This creates uncertainties in selecting and evaluating soil health indicators for minimizing N_2O emissions, posing a threat to the environment and contributing to emissions and climate change. Hence, the present study aimed to assess the impact of the pore structural functionality and architecture on N_2O diffusion under contrasting soil structural states at different depths.

2. Material and methods

2.1. Site and management

Soil samples were taken from a compaction experiment, with known management history, at a lysimeter semi-field facility at the Lucio Toniolo experimental farm of the University of Padua (45°19′ N, 11°31′ E, 8 m above sea level), low plain Veneto region, Italy. The soil in the freely draining concrete lysimeters (1 m length × 1 m width × 1.5 m depth) was a Fluvi-Calcaric Cambisol (IUSS-WorkingGroup-WRB et al., 2015) with a silt loam texture, and soil total nitrogen and organic carbon contents (at sampling) ranging between 0.6 and 1.0 g kg^{-1} and 5.3–7.8 g kg^{-1}, respectively (Table 1).

Prior to the present experiment, as described by Longo et al. (2021) the lysimeters were used for assessing the effects of groundwater levels, fertiliser rates (2011–2015), fertiliser types (2015), and farming systems (conventional and conservation agriculture) (since 2016) on greenhouse gases. From 2011, maize (*Zea mays* L.) was the main crop grown, except in 2019 and 2020 when sorghum (*Sorghum bicolor* L.) and winter wheat (*Triticum aestivum* L.) were sown, respectively. As is commonly practised in the region, conventional agriculture involved tillage, residue incorporation after crop harvesting, and bare soil during winter, whereas conservation agriculture was characterised by no-tillage, and cover crops during winter and summer i.e., from 2016 to 2020, respectively, forage radish (*Raphanus sativus* L.), forage sorghum [Sorghum × drummondii (Nees ex Steud.) Millsp. & Chase], forage radish, ryegrass (*Secale cereale* L.), and sudan grass (Sorghum × drummondii) (Longo et al., 2021).

2.2. Experimental design

For the present study, soil sampling was conducted in lysimeters under conservation agriculture with previously simulated topsoil or subsoil compaction (applied on May 30, 2022), and uncompacted lysimeters under conventional management. The experimental design included three treatments in a completely randomised design with four replicates. The treatments were: topsoil compaction (TopComp), subsoil compaction (SubComp) and no compaction (NoComp).

In the lysimeters for the NoComp treatment included, the top 25 cm depth being tilled by hand spading. In the TopComp, compaction was conducted in the 0–25 cm layer. This soil layer was excavated, prewetted and then returned to the lysimeter by compressing fine layers of about 3 cm, one at a time, aiming for a bulk density of ca.1.6 Mg m^{-3}. The same procedure was followed to compact the 25–45 cm soil layer in the SubComp treatment, while the 0–25 cm depth soil was returned without compression. Bulk density after compaction was not determined because of limited capacity for multiple samplings in the lysimeters. This

Table 1
Soil mineral particle content, inorganic and organic carbon, and total nitrogen of the studied silt loam soil.

Depth (cm)	Treatment	Clay (<2 μm) g kg^{-1}	Silt (2–50 μm) g kg^{-1}	Sand (50–2000 μm) g kg^{-1}	Organic Carbon g kg^{-1}	Inorganic Carbon g kg^{-1}	Total Kjeldahl Nitrogen g kg^{-1}
10–20	NoComp	191 ± 12	535 ± 7 AB	274 ± 8	7.6 ± 0.03	40.4 ± 0.05	0.9 ± 0.04
	TopComp	201 ± 12	528 ± 7 A	271 ± 7	7.3 ± 0.03	41.9 ± 0.09	0.9 ± 0.04
	SubComp	207 ± 12	546 ± 7 AB	247 ± 18	7.8 ± 0.03	41.1 ± 0.02	1.0 ± 0.04
30–40	NoComp	202 ± 12	531 ± 7 A	267 ± 8	6.2 ± 0.03	40.9 ± 0.04	0.7 ± 0.04
	TopComp	174 ± 13	529 ± 8 AB	297 ± 11	5.3 ± 0.03	43.8 ± 0.23	0.6 ± 0.04
	SubComp	201 ± 12	529 ± 7 A	270 ± 7	6.2 ± 0.03	407 ± 0.03	0.8 ± 0.04
50–60	NoComp	237 ± 12	583 ± 7 C	180 ± 17	6.0 ± 0.03	40.7 ± 0.02	0.8 ± 0.04
	TopComp	204 ± 13	602 ± 8 C	194 ± 26	5.9 ± 0.03	40.6 ± 0.03	0.7 ± 0.04
	SubComp	215 ± 12	567 ± 7 BCE	218 ± 18	5.9 ± 0.03	41.2 ± 0.05	0.7 ± 0.04
P-value	*Treatment*	*0.231*	*0.867*	*0.305*	*0.326*	*0.671*	*0.267*
	Depth	*0.040*	*<0.001*	*<0.001*	*<0.001*	*0.844*	*<0.001*
	Treat × Depth	*0.305*	*0.038*	*0.108*	*0.541*	*0.265*	*0.501*

NoComp is soil without compaction treatment, TopComp is soil with topsoil compaction treatment, and SubComp is soil with subsoil compaction treatment. Values are means with standard error (n = 4). *Treat × Depth* is the interaction of treatment and depth. Values in a column followed by a different lowercase letter significantly differ across treatments within the same depth, and uppercase letters show differences across treatments and depth, at a 5% significance level.

precaution was taken to prevent the formation of preferential pathways within the lysimeters.

All the lysimeters received, 46 days after soil compaction (July 15, 2022), a mixed animal-vegetable solid digestate, obtained from a local biogas plant, which was incorporated at 0–5 cm depth at a rate of 315.2 kg N ha^{-1}. Maize was sown at a density of 8 plants m^{-2} three days after the application of digestate. The water table level was kept constant throughout the experiment at 120 cm depth.

2.3. Soil sampling and measurements pre-incubations

After crop harvest (122 days after sowing), intact soil core samples of 226 cm^3 (using aluminium rings of 6.0 cm diameter, 8.0 cm height) were taken, vertically, from each lysimeter at 10–20, 30–40 and 50–60 cm depths, giving a total of 36 samples.

The intact soil cores were placed on tension tables, saturated from below, and then drained stepwise to soil water matric potentials of −30, −50 and −100 h Pa. At each matric potential, air permeability (k_a) and gas diffusivity were measured sequentially. Quantification of k_a was based on the Forchheimer approach using an apparatus that allows automatic measurement of airflow at four pneumatic pressures of around 5, 2, 1, and 0.5 hPa (Schjønning and Koppelgaard, 2017). The relative gas diffusivity (D_s/D_o, where D_s and D_o are gas diffusion coefficients in soil and free air, respectively), was derived using the steady-state diffusion approach, and measurements were conducted by using the one-chamber one-gas method (Schjønning et al., 2013).

The air-filled pore space (ε_a) and the WFPS were calculated using the mass water balance at each matric potential. Total porosity was estimated from dry bulk density (ρ_b) and particle density. The latter was estimated using a function proposed by Schjønning et al. (2017) that includes clay and soil organic matter contents as predicting variables; readers are referred to equation 10 in that study.

Further characterisation of the soil pore network was conducted using the relationship between the k_a and ε_a, denoted as PO1 (Groenevelt et al., 1984), and by the calculation of soil pore geometry indices such as tortuosity and effective pore diameter (d_{eff}) (Ball, 1981).

In addition, along with the intact soil core samples, disturbed soil samples were simultaneously collected to determine sand, silt, and clay content (particle size analyzer Mastersizer 2000; Malvern Panalytical Ltd, Spectris Company), organic and inorganic carbon content (elemental analyzer VARIO MACRO; Elementar Analysensysteme GmbH), and total nitrogen content (Kjeldahl method). Moreover, the degree of compactness was determined by calculating the reference bulk density value using a model which considers both soil particles (sand, silt, clay) and soil organic matter contents, equation 12 in Keller and Håkansson (2010).

2.4. Micro CT-image acquisition, processing, and analysis

Intact soil samples equilibrated at a soil matric potential of −100 h Pa were scanned using a micro-X-ray computed microtomography (μCT) equipment (EasyTom XL 160/230 Mechanic Ultra, RX solutions device) at the University of Padua. The scanning of soil samples was performed at a voltage of 199 kV and a beam current of 202 μA, which set the tube power to 40 W. The reconstruction of the acquired images was achieved through the filtered back projection method, obtaining 3D tomographs with 40 × 40 × 40 μm voxel size and 16-bit grey scale.

The digital image processing and analysis were performed using the open-source software ImageJ2/Fiji (Rueden et al., 2017). A soil volume of interest, 50 mm in diameter and 60 mm in height, was selected to avoid boundary effects. To reduce noise, the images were normalised with a saturated pixel of 0.4% and filtered with the Non-Local Means Denoising filter (parameters were set to auto sigma value and a smoothing factor of 1) (Buades et al., 2011). The segmentation of the image was performed using the Moments method (Tsai, 1985). Isolated segmentation noise in the images was removed by the morphological closing operation (disregarding pores with a volume smaller than two voxels).

The "Particle Analyser" module of the BoneJ plugin (Doube, 2021) and the "Analyse Skeleton (2D/3D)" plugin were used to obtain μCT-derived parameters for the characterisation of the visible macropore morphology: total macroporosity, macropore density, mean macropore diameter (mean of Local Thickness values weighted by frequency within the volume of interest), Euler density, total branch length, and largest macropore ratio (volume of largest macropore/total macroporosity). The three latter parameters were used as pore connectivity indicators. The μCT-derived volume of the macropores connected to the upper and bottom ends of the sample was also quantified (Koestel and Schlüter, 2019).

Additionally, the Euclidean distance transform plugin was used to estimate the Euclidean distance to the closest pore in the soil matrix (Euclidean distance values weighted by frequency within the volume of interest) (Schlüter and Vogel, 2016). This parameter, named hereafter solid-to-pore distance, was used as an indicator of the travel distance of gases to pores where exchanges with the rest of the soil profile take place (Kravchenko and Guber, 2021).

2.5. Laboratory incubations and measurements

After the equilibration at each matric potential, and subsequent to gas diffusivity measurement, soil cores were used for an incubation experiment. Firstly, soil cores were placed between a polyvinyl chloride (PVC) top and a bottom compartment, each of 135 cm^3, which

functioned as headspace and gas reservoir, respectively. Each compartment had two rubber septa, which facilitated the sealing and gas sampling. Air tightness of each unit was first tested by immersion in water after applying an overpressure of 60 ml, which was greater than the gas pressure applied during the tests with soil cores.

After closing the headspace and gas reservoir compartments, containing ambient air, a gas sample was taken from the headspace about 14 h after closing to determine the background concentration of N_2O, [N_2O], emitted from the soil. Then, each bottom reservoir received 0.5 mL of a 1% N_2O gas mixture (1% N_2O, 99% N_2) via a septum to increase [N_2O] in the reservoir from ambient (0.32 μL N_2O L^{-1}) to 30 μL N_2O L^{-1}. Monitoring of headspace [N_2O] was conducted by taking a 4 mL gas sample at 1, 2, 3, 6, 10, 24, and 30 h after the injection of N_2O into the bottom reservoir. After each gas sampling, an aliquot of ambient air, equivalent to the volume withdrawn, was injected into the headspace to avoid pressure change. Ambient air [N_2O] was determined twice per day. Ambient air and soil background [N_2O] were deducted from the [N_2O] accumulating in the headspace. After the last sampling from the headspace, a gas sample was also taken from the reservoir to determine residual [N_2O].

Following the final gas sampling at −100 h Pa, each soil core was manually extruded into a Ziploc® bag, which was immediately sealed. The soil core was then manually fragmented inside the closed bag, and a gas sample was collected from the air volume inside the bag to determine any N_2O entrapped in the soil. The volume of gas inside the Ziploc® bag was determined by placing the bag in water and measuring the displacement of water, with the gas volume calculated by subtracting the volume of soil and water of the soil core.

A gas chromatography system was utilized to determine the concentration of N_2O and carbon dioxide (CO_2) of the gas samples. Details can be found in Petersen et al. (2012).

The diffusion of N_2O through the intact soil cores was determined by assessing its rate of accumulation in the headspace and the remaining concentration in the reservoir. The [N_2O] that was entrapped in the air-filled pore space and dissolved in the soil solution was calculated following (Davidson and Firestone, 1988). This involved the use of the soil mass and the Bunsen solubility coefficient in water (0.622, at 21 °C), respectively. The Bunsen coefficient accounts for N_2O dissolved in the liquid phase of the soil cores assuming equilibrium between headspace and liquid phases.

The incubations and all physical measurements were conducted at a controlled room temperature of 21 °C degrees.

2.6. Soil analyses after incubations

Subsamples were taken from the fragmented soil cores to determine soil moisture content, concentrations of ammonium, [NH_4] and nitrate [NO_3], and hot-water extractable organic carbon (HWEC). Soil NH_4 and NO_3 were extracted with 1 M KCl at a ratio of 1:4 (soil: extractant), and determined on an auto-analyser (AA500, Seal Analytical, 22803 Norderstedt, Germany). The HWEC was determined using the hot-water extraction method with a 1:10 soil-to-water ratio (Ghani et al., 2003). The method involved first an extraction with cold water (readily water-soluble C) followed by hot water extraction (labile C) at 80 °C for 16 h. The total carbon concentration of both extractions was determined on a Shimadzu total organic carbon (TOC) analyser (Shimadzu Corporation, Kyoto, Japan).

Another soil subsample was air-dried to determine soil pH (1:2.5 soil-to-water ratio) and electrical conductivity (1:5 soil-to-water ratio). The *nosZ* gene, which codes for N_2O reductase in the denitrification pathway, was also quantified. The extraction of DNA from soils was conducted using the Qiagen DNeasy PowerSoil Pro kit Kit (Qiagen, Hilden, DE) as described by the manufacturer's protocol on 0.4 g of air-dried samples. The extracted DNA was quantified with a Qubit 3.0 fluorimeter (Thermo Fisher Scientific, Carlsbad, CA) using the Qubit™ DNA HS Assay Kit (Thermo Fisher Scientific, Carlsbad, CA) and stored at −20 °C. Quantitative real-time PCR was conducted using the primer pair *nosZ* F 5′ CGYTGTTCMTCGACAGCCAG 3′, and *nosZ* R 5′ CATGTGCAGNGCRTGGCAGAA 3' (Rösch et al., 2002). A QuantStudio 5 System (Life Technologies, Carlsbad, CA) was used to perform the qPCR analyses in a final 5 μL reaction volume. The thermal conditions for each qPCR corresponded to a pre-denaturing stage at 95 °C for 10 min, followed by 40 cycles with denaturation step at 95 °C for 15 s, annealing step at 57 °C for 60 s and extension at 72 °C for 60 s. The Ct threshold cycles values were transformed into gene copies using the equation by Dong et al. (2020a).

2.7. Statistical analyses

Regression analysis was conducted to evaluate the effects of treatment × depth × matric potential or treatment × depth interaction for the studied variables. Linear and generalized linear mixed models (glmmTMB) were fitted according to the nature of the response variable, using gaussian or gamma distribution with identity or logarithmic link to achieve better model fits. ANOVA was performed to assess model significance. The 'emmeans' package was utilized to calculate marginal means for the interaction and main effects. Tukey's HSD method was used for multiple comparisons. Additionally, a Spearman's rank correlation test was conducted between each pair of variables. These analyses were performed using the statistical package R (Team-RDC, 2021). All tests were conducted at the 5% significance level.

Decision trees were built to further select interacting factors driving N_2O diffusion in the soil layers. First, regression trees were built to predict the ratio of N_2O diffusion (N_2O in the headspace/N_2O injected into the reservoir) for the combined data set (all depths and matric potentials). Then, the dataset at −100 h Pa was used to build a regression tree, for which the input variables included measured and μCT-derived parameters. Principal component analysis was used to reduce data dimension (data not shown). The reduced input variables were ρ_b, ε_a, k_a, D_s/D_o, WFPS, Euler density, total branch length, largest macropore ratio, solid-to-pore distance, and connected macropores ratio. Additionally, classification trees were generated to assess the variables that best explained the level of N_2O diffusion. The level of N_2O diffusion was classified as low or high according to the 25th and 75th percentile scores of the data, respectively. Moderate level was considered for N_2O diffusion ratios that fell in between the 25th and 75th percentile. Models were built with a 10-fold cross-validation, a pruning confidence factor of 0.25 and binary splits. Decision trees were built with the Waikato Environment for Knowledge Analysis (WEKA) using the J48-C4.5 algorithm for classification trees and the M5 algorithm for model trees (Hall et al., 2009).

3. Results

3.1. Soil structure-related parameters and pore functionality

The mean ρ_b of intact soil cores ranged from 1.40 to 1.59 Mg m^{-3}, with a significant interaction between treatment and depth ($P = 0.012$) (Table 2). At 10–20 cm depth, TopComp had a higher ($P = 0.020$) ρ_b value of 1.58 Mg m^{-3} compared to the SubComp, and NoComp (1.40 and 145 Mg m^{-3}, respectively). Correspondingly, the TopComp exhibited a significantly larger degree of compactness and lower total porosity (96% and 0.41 m^3 m^{-3}, respectively) compared to SubComp for 10–20 cm depth (87% and 0.47 m^3 m^{-3}, respectively). The SubComp for 50–60 cm depth was compacted as SubComp for 10–20 cm ($P < 0.01$). No treatment effect was found for ρ_b, total porosity, and degree of compactness for 30–40 cm.

For soil pore parameters, there was no significant interaction effect for treatment × depth × matric potential, but a significant treatment × depth interaction occurred ($P = 0.001$) (Tables 3 and 4). The greatest contrasting conditions were found for 10–20 cm depth, where the TopComp showed very low ε_a (0.02–0.03 m^3 m^{-3}), k_a (0.1–0.3 μm^2),

Table 2
Soil bulk density, degree of compactness and total porosity of the studied silt loam soil.

Depth (cm)	Treatment	Bulk density (Mg m^{-3})	Degree of compactness (%)	Total porosity (m^3 m^{-3})
10–20	NoComp	1.45 ± 0.03 a AB	89 ± 2 AB	0.45 ± 0.01 BCE
	TopComp	1.58 ± 0.03 b BC	96 ± 2 BCE	0.41 ± 0.01 AB
	SubComp	1.40 ± 0.03 a A	87 ± 2 A	0.47 ± 0.01 C
30–40	NoComp	1.49 ± 0.03 a ABC	91 ± 2 ABC	0.44 ± 0.01 ABC
	TopComp	1.54 ± 0.03 a ABC	93 ± 2 ABC	0.42 ± 0.01 ABC
	SubComp	1.50 ± 0.03 a ABC	91 ± 2 ABC	0.44 ± 0.01 ABC
50–60	NoComp	1.52 ± 0.03 a ABC	95 ± 2 BCE	0.43 ± 0.01 ABC
	TopComp	1.54 ± 0.03 a BC	97 ± 2 BCE	0.42 ± 0.01 ABC
	SubComp	1.59 ± 0.03 a C	99 ± 2 C	0.40 ± 0.01 A
P-value	*Treatment*	*0.020*	*0.021*	*0.018*
	Depth	*0.006*	*<0.001*	*0.011*
	Treat × Depth	*0.012*	*0.041*	*0.013*

NoComp is soil without compaction treatment, TopComp is soil with topsoil compaction treatment, and SubComp is soil with subsoil compaction treatment. Values are means with standard error (n = 4). *Treat × Depth* is the interaction of treatment and depth. Values in a column followed by a different lowercase letter significantly differ across treatments within the same depth, and uppercase letters show differences across treatments and depth, at a 5% significance level.

and D_s/D_o (0.001–0.002) values, and a very high WFPS (93–96%) compared to NoComp and SubComp across matric potentials ($P < 0.001$) (Table 3). Concomitantly, compaction tended to increase tortuosity for TopComp and significantly reduced the effective pore diameter (d_{eff}) and PO1 (k_a/ε_a) at all three matric potentials ($P < 0.001$) (Table 4).

There was a significant treatment × depth interaction for all CT-derived parameters ($P < 0.001$ – $P = 0.031$), except for mean diameter. A distinct treatment effect occurred for 10–20 cm depth where TopComp had lower macroporosity volume, lower pore connectivity (i.e., 2.6–2.8 times lower values of largest-macropore ratio and 3–5 times less macropore branching), and larger solid-to-pore distance when compared to SubComp and NoComp treatments (Fig. 1). For 30–40 cm depth, SubComp had larger pore density, smaller mean diameter, and lower solid-to-pore distance than TopComp ($P < 0.05$). The connected macropores ratio (μCT-derived end-to-end connected macropore volume) accounted for 0.76–0.94 of total μCT-macroporosity for 10–20 cm, except in the TopComp treatment, where it was only 0.25 and significantly lower than in NoComp and SubComp ($P < 0.05$) (Fig. 1).

3.2. Nitrous oxide recoveries

The background concentration of N_2O, [N_2O], emitted from the soil before the injection of N_2O was generally lower than the ambient concentration, with values ranging from −0.12 to 0.37 μL L^{-1} at −30 h Pa, −0.09 to 1.18 μL L^{-1} at −50 h Pa, and −0.06 to 0.789 at −100 h Pa (data not shown).

Table 3
Soil pore characteristics of the studied silt loam soil at different soil water matric potentials and soil depths: air-filled pore space (ε_a), water-filled pore space (WFPS), air permeability (k_a), and relative gas diffusivity (D_s/D_o).

Depth (cm)	Treatment	−30 hPa				−50 hPa				−100 hPa			
		ε_a (m^3 m^{-3})	WFPS (%)	k_a (μm^2)	D_s/D_o × 1000	ε_a (m^3 m^{-3})	WFPS (%)	k_a (μm^2)	D_s/D_o × 1000	ε_a (m^3 m^{-3})	WFPS (%)	k_a (μm^2)	D_s/D_o × 1000
10–20	NoComp	0.11 ± 0.02 CD	76 ± 3 A	43.0 ± 20.2 C	7.9 ± 2.2 BCE	0.12 ± 0.02 CD	73 ± 3 A	38.2 ± 17.9 CD	9.3 ± 2.2 CD	0.14 ± 0.02 CD	70 ± 3 A	46.3 ± 21.7 BCE	12.8 ± 2.2 B
	TopComp	0.02 ± 0.005 A	96 ± 2 D	0.1 ± 0.1 A	1.6 ± 0.6 AB	0.03 ± 0.005 A	95 ± 2 D	0.3 ± 0.3 A	0.9 ± 0.6 A	0.03 ± 0.01 A	93 ± 2 D	0.3 ± 0.3 A	1.7 ± 0.6 A
	SubComp	0.11 ± 0.02 D	76 ± 3 A	58.8 ± 35.5 C	11.1 ± 5.6 C	0.13 ± 0.01 D	72 ± 3 A	98.2 ± 59.3 D	17.2 ± 5.6 D	0.15 ± 0.01 D	68 ± 3 A	150.3 ± 90.8 C	23.6 ± 5.6 B
30–40	NoComp	0.10 ± 0.02 CD	78 ± 4 AB	13.9 ± 3.5 BCE	4.9 ± 1.6 ABC	0.11 ± 0.02 BCD	76 ± 4 AB	11.8 ± 2.9 BCE	5.1 ± 1.6 BCD	0.13 ± 0.02 BCD	72 ± 4 AB	14.0 ± 3.5 B	7.7 ± 1.6 AB
	TopComp	0.07 ± 0.02 ABCD	83 ± 4 ABCD	39.1 ± 25.1 BCE	6.3 ± 3.7 ABC	0.08 ± 0.02 ABCD	81 ± 4 ABCD	20.0 ± 12.8 BCD	6.7 ± 3.7 ABCD	0.10 ± 0.02 ABCD	77 ± 2 ABC	26.7 ± 17.2 BCE	9.7 ± 3.7 AB
	SubComp	0.07 ± 0.01 CD	84 ± 2 AB	8.8 ± 5.2 BCE	5.3 ± 2.6 ABC	0.08 ± 0.01 BCD	82 ± 2 AB	25.6 ± 17.7 BCD	7.9 ± 2.6 CD	0.10 ± 0.01 BCD	78 ± 2 AB	43.3 ± 25.9 BCE	13.3 ± 2.7 B
50–60	NoComp	0.05 ± 0.004 BCE	88 ± 1 BCE	4.7 ± 2.9 BCE	2.6 ± 0.4 A	0.07 ± 0.004 BCE	85 ± 1 BCE	4.2 ± 2.6 ABC	2.7 ± 0.4 AB	0.08 ± 0.004 BCE	82 ± 1 B	5.2 ± 3.1 AB	3.8 ± 0.4 A
	TopComp	0.04 ± 0.01 ABC	90 ± 2 BCD	6.2 ± 1.4 B	3.4 ± 0.6 A	0.05 ± 0.01 AB	88 ± 2 BCD	8.6 ± 1.9 BCE	4.9 ± 0.6 C	0.07 ± 0.01 AB	84 ± 2 BCD	13.4 ± 2.9 B	8.8 ± 0.6 B
	SubComp	0.02 ± 0.01 AB	95 ± 2 CD	4.8 ± 1.8 B	2.4 ± 1.1 A	0.03 ± 0.01 A	93 ± 2 CD	5.7 ± 2.1 AB	3.3 ± 1.1 ABC	0.04 ± 0.01 A	90 ± 2 CD	10.2 ± 3.8 AB	6.9 ± 1.1 AB
P-value	*Treat × Depth*	*<0.001*	*<0.001*	*<0.001*	*<0.001*								
	Treat × Ψ	*0.978*	*0.988*	*0.599*	*0.212*								
	Depth × Ψ	*0.989*	*0.999*	*0.996*	*0.976*								
	Treat × Depth × Ψ	*0.989*	*0.999*	*0.927*	*0.913*								

NoComp is soil without compaction treatment, TopComp is soil with topsoil compaction treatment, and SubComp is soil with subsoil compaction treatment. *Treat × Depth × Ψ* is the interaction of treatment (*Treat*), depth and soil water matric potential (*Ψ*). Values are means with standard error (n = 4). Values in a column followed by different uppercase letters show differences across treatments and depth, at a 5% significance level.

Table 4
Pore geometry indices derived from the tube model (tortuosity and effective pore diameter, d_{eff}) and the ratio of air permeability (k_a) and air-filled pore space (ε_a), denoted as PO1. All indices were estimated at three soil water matric potentials.

Depth (cm)	Treatment	−30hPa			−50hPa			−100hPa		
		Tortuosity	d_{eff} (μm)	PO1 (μm^2)	Tortuosity	d_{eff} (μm)	PO1 (μm^2)	Tortuosity	d_{eff} (μm)	PO1 (μm^2)
10–20	NoComp	3.9 ± 0.3 AB	362.2 ± 50.8 B	326 ± 114 B	3.8 ± 0.3 AB	314.5 ± 50.8 B	255 ± 89 AB	3.5 ± 0.3 AB	289.8 ± 50.8 B	272 ± 115 BCD
	TopComp	6.8 ± 1.2 AB	19.6 ± 23.1 A	3 ± 3 A	5.6 ± 1.2 ABC	45.6 ± 23.1 A	9 ± 10 A	5.0 ± 1.2 ABC	31.1 ± 23.1 A	7 ± 6 A
	SubComp	4.1 ± 0.5 AB	267.5 ± 55.1 B	374 ± 200 B	3.3 ± 0.5 ABC	373.4 ± 55.1 B	635 ± 339 B	2.8 ± 0.5 ABC	392.3 ± 55.1 B	882 ± 272 D
30–40	NoComp	4.6 ± 0.2 B	292.8 ± 13.4 B	133 ± 17 B	4.8 ± 0.2 BCE	285.1 ± 13.4 B	108 ± 14 A	4.2 ± 0.2 BCE	237.8 ± 13.4 B	105 ± 15 AB
	TopComp	3.9 ± 0.7 AB	419.6 ± 70.0 B	505 ± 263 B	4.8 ± 0.7 ABC	268.7 ± 70.0 AB	178 ± 93 AB	3.8 ± 0.7 ABC	263.9 ± 70.0 AB	226 ± 136 ABCD
	SubComp	3.8 ± 0.6 AB	172.7 ± 48.3 AB	119 ± 67 B	3.9 ± 0.6 ABC	271.3 ± 55.8 B	295 ± 191 AB	3.1 ± 0.6 ABC	241.7 ± 48.3 B	396 ± 141 BCD
50–60	NoComp	4.6 ± 0.3 B	186.8 ± 40.6 B	82 ± 49 AB	5.1 ± 0.3 C	205.5 ± 40.6 B	62 ± 36 AB	4.7 ± 0.3 C	186.7 ± 40.6 B	61 ± 23 ABC
	TopComp	3.4 ± 0.3 AB	233.9 ± 22.2 B	150 ± 22 B	3.3 ± 0.3 A	235.6 ± 22.2 B	164 ± 24 AB	2.8 ± 0.3 A	221.8 ± 22.2 B	219 ± 31 CD
	SubComp	3.0 ± 0.3 A	243.3 ± 24.1 B	211 ± 55 B	3.0 ± 0.3 A	214.5 ± 24.1 B	163 ± 42 AB	2.6 ± 0.3 A	299.2 ± 79.9 B	299 ± 155 CD
P-value	*Treat × Depth*	*<0.001*	*<0.001*	*<0.001*						
	Treat × Ψ	0.606	0.851	0.58						
	Depth × Ψ	*0.580*	*0.767*	*0.977*						
	Treat × Depth × Ψ	*0.991*	*0.333*	*0.696*						

NoComp is soil without compaction treatment, TopComp is soil with topsoil compaction treatment, and SubComp is soil with subsoil compaction treatment. Tortuosity $= [\varepsilon_a/(D_s/D_o)]^{1/2}$; effective diameter ($d_{eff}$) $= 2[(8\ k_a)/D_s/D_o]^{1/2}$; PO1 $= k_a/\varepsilon_a$. *Treat* × *Depth* × *Ψ* is the interaction of treatment (*Treat*), depth and soil water matric potential (*Ψ*). Values are means with standard error (n = 4). Values in a column followed by different uppercase letters show differences across treatments and depth, at a 5% significance level.

Fig. 2 displays changes in the N_2O diffusion ratio, which is the ratio of N_2O detected in the headspace to the N_2O injected into the reservoir. This ratio increased in the first 6 h with a maximum between 10 and 24 h after the N_2O injection, regardless of matric potential. However, for 10–20 cm depth, the N_2O diffusion ratio increased at a much slower rate in the TopComp than in the SubComp and NoComp, at all three matric potentials.

There was no significant interaction effect between treatment × depth × matric potential or treatment × matric potential ($P > 0.05$) for cumulative N_2O detected in neither the headspace nor the reservoir (Fig. 3). For 10–20 cm soil depth, TopComp had on average a 7% N_2O diffusion ratio while in the SubComp and NoComp it was 2.4–3.4 (17–24%) times higher ($P < 0.001$), across the three matric potentials (Fig. 3). For 30–40 cm and 50–60 cm depths the N_2O diffusion ratio ranged from 17 to 23% across treatments and matric potentials. Some of the injected N_2O remained in the reservoir 30 h after the injection (Fig. 3). For 10–20 cm depth, the N_2O ratio in the reservoir (N_2O remaining/N_2O injected) was higher for TopComp (32–45%) compared to SubComp (17–22%) and NoComp (16–25%) across matric potentials ($P < 0.001$), except at −100 h Pa that only differ from NoComp.

At −100 h Pa, the estimated N_2O entrapped in the air-filled pore space and dissolved in soil water corresponded to, respectively, 16–35% and 9–21% of the initial N_2O injection (Table 5). These N_2O recovered fractions were not significantly affected by treatment ($P > 0.05$). It was assumed that the N_2O not recovered (difference between the injected and the recoveries in soil air and water) was reduced to N_2, which was not significantly affected by treatment.

Additionally, Fig. 2 depicts the changes in the headspace [CO_2] across treatments, soil depths, and matric potentials following the injection of N_2O. The [CO_2] detected seemed to decrease with depth for all treatments regardless of soil water matric potential. Cumulative [CO_2] was higher in the TopComp and SubComp compared to NoComp at −30 h Pa ($P < 0.001$).

3.3. HWEC, NH_4, NO_3, *nosZ* gene, pH and electrical conductivity

At the end of the experiment, at −100 h Pa, the soil had varying levels of HWEC (354–528 μg C g^{-1} soil), NH_4–N (0.08–0.80 μg g^{-1} soil), and NO_3–N (0.27–5.62 μg g^{-1} soil), which tended to decrease with depth (Table 6). In general, no significant differences were observed for these parameters between compaction treatments, except for a lower NO_3–N concentration ($P = 0.039$) for TopComp compared to SubComp for 10–20 cm. Additionally, as shown in Supplementary Table A, NO_3–N had a negative correlation with ρ_b ($r = -0.367$, $P = 0.05$) and degree of compactness ($r = -0.505$, $P = 0.01$) and a positive correlation with k_a, D_s/D_o, d_{eff} and PO1 ($r = 0.388$–0.452, $P = 0.01$–0.05). Whereas NH_4–N was negatively correlated with degree of compactness ($r = -0.345$, $P = 0.05$).

The number of *nosZ* copies was significantly higher in the SubComp compared to NoComp for all three depths ($P = 0.023$) (Table 6). The *nosZ* copies were significantly correlated to HWEC ($r = 0.463$, $P = 0.01$), NH_4–N ($r = 0.486$, $P = 0.01$) and tortuosity ($r = -0.442$, $P = 0.05$). Furthermore, [CO_2] at −100 h Pa was positively correlated with HWEC, NH_4–N, NO_3–N, and *nosZ* copies ($r = 0.477$–$0{,}716$, $P = 0.01$) (Supplementary Table A).

Soil pH (7.89–8.09), and electrical conductivity (142–198 μS cm^{-1}), showed no significant differences between treatments and depths (Table 6).

3.4. Explanatory variables of N_2O diffusion

Spearman correlation tests, across factors, showed significant ($P < 0.01$) positive correlations between the N_2O diffusion ratio and ε_a, k_a, D_s/D_o, d_{eff} and PO1 ($r = 0.407$ to 0.520), and significant ($P < 0.01$) negative correlations with WFPS, and tortuosity ($r = -0.396$ to -0.281) (Supplementary Table B). The N_2O diffusion ratio was significantly ($P < 0.05$) correlated to ρ_b and total pore volume at both −30 and −100 h Pa, and to degree of compactness at −100 h Pa (Supplementary Table C).

Fig. 4 illustrates the N_2O diffusion ratio as a function of pore structural-related parameters across treatments, depths, and matric

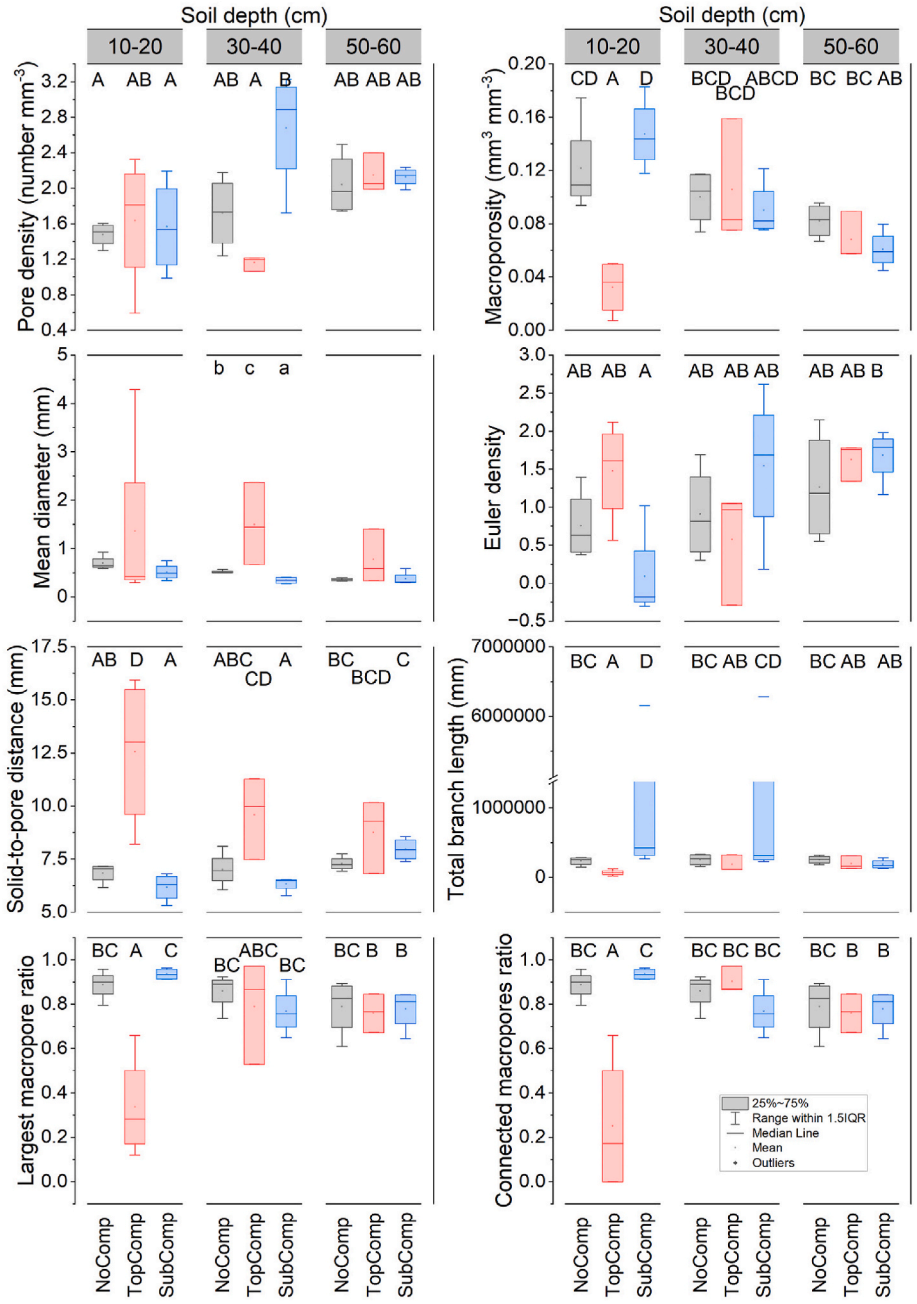

Fig. 1. X-ray Computed Tomography-derived soil pore parameters of the studied silt loam soil. NoComp is soil without compaction treatment, TopComp is soil with topsoil compaction treatment, and SubComp is soil with subsoil compaction treatment. Boxes followed by a different lowercase are significantly different among treatments within the same depth. Uppercase letters show the treatment × depth interaction, at a 5% significance level.

potentials. Nitrous oxide diffused through the intact soil cores with D_s/D_o ranging from 0.002 to 0.045, and at WFPS ranging from 60 to 99% across matric potential. Fig. 4 also suggests that k_a, d_{eff} and PO1 better explained the variation in N_2O diffusion ratio, by a higher coefficient of determination (r^2 = 0.63–0.65), than WFPS, D_s/D_o and tortuosity (r^2 = 016 0.29) for the present dataset.

Significant correlations ($P < 0.05$) between the N_2O diffusion ratio, N_2O in soil air and N_2O in soil water and the μCT-derived parameters (Supplementary Table A) suggest that at −100 h Pa, a dense soil matrix with a pore network characterised by low macroporosity and simple architecture (poor branching and isolated pores) contributed to less N_2O diffusing into the headspace and promoted entrapment of N_2O in air-filled pores and water in the soil core.

From our dataset, the first generated regression tree predicted the N_2O diffusion ratio from only the variables measured at the three matric potentials (WFPS, k_a, D_s/D_o and N_2O diffusion ratio). A one-rule model was built with WFPS and k_a as predictor variables, with a correlation coefficient of 0.73, root mean squared error of 0.21 and n = 101:

$$log_{10}N_2O\_diffussionRatio = 0.8447WFPS + 0.2212\, log_{10}k_a - 1.6316 \quad (1)$$

Then, when only parameters measured at −100 h Pa (ε_a, k_a, D_s/D_o, WFPS, Euler density, total branch length, largest macropore ratio, solid-to-pore distance, and connected macropores ratio) and ρ_b were considered, a one-rule model was also generated to predict N_2O diffusion ratio, with only the largest macropore ratio as a predicting variable and an acceptable predictive power (correlation coefficient of 0.64, root mean squared error of 0.23 and n = 34):

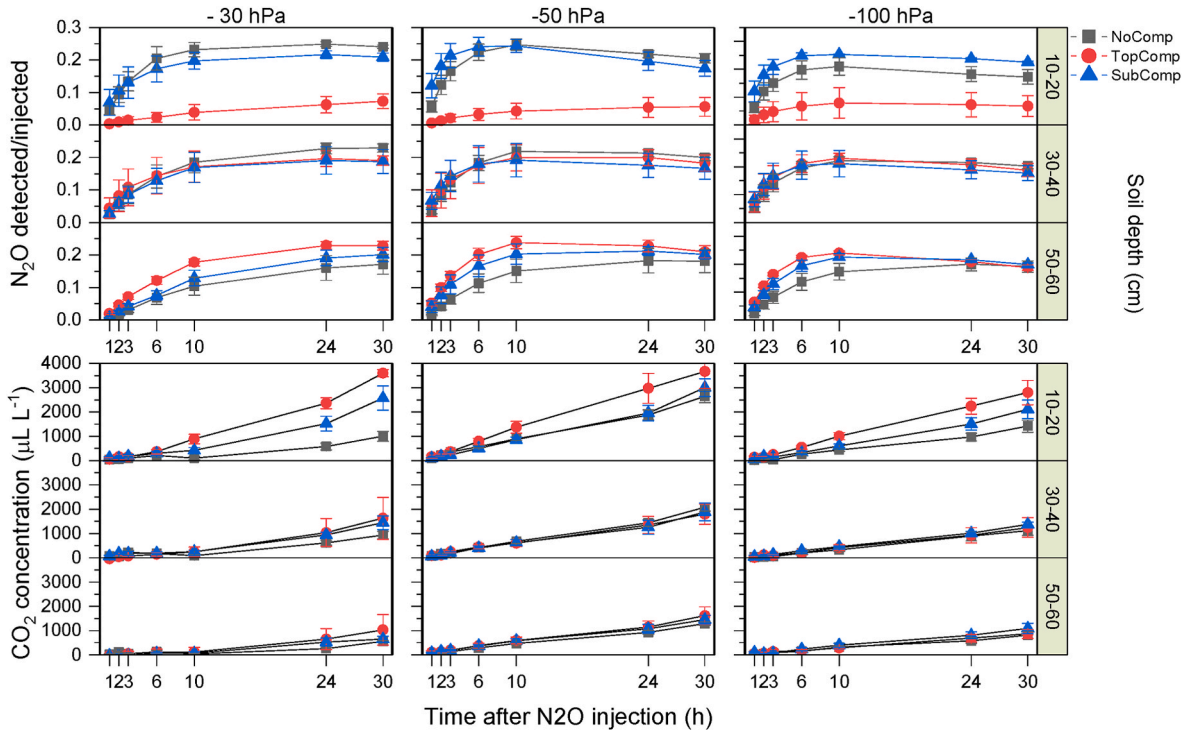

Fig. 2. Changes in the nitrous oxide (N_2O) relative to the injected N_2O, as well as changes in carbon dioxide (CO_2), detected in the headspace over a 30-h period following the injection of N_2O into the reservoir. Data points represent the mean values at different treatments, soil water matric potentials and soil depths. NoComp is soil without compaction treatment, TopComp is soil with topsoil compaction treatment, and SubComp is soil with subsoil compaction treatment. Error bars denote the standard error of the mean (n = 4).

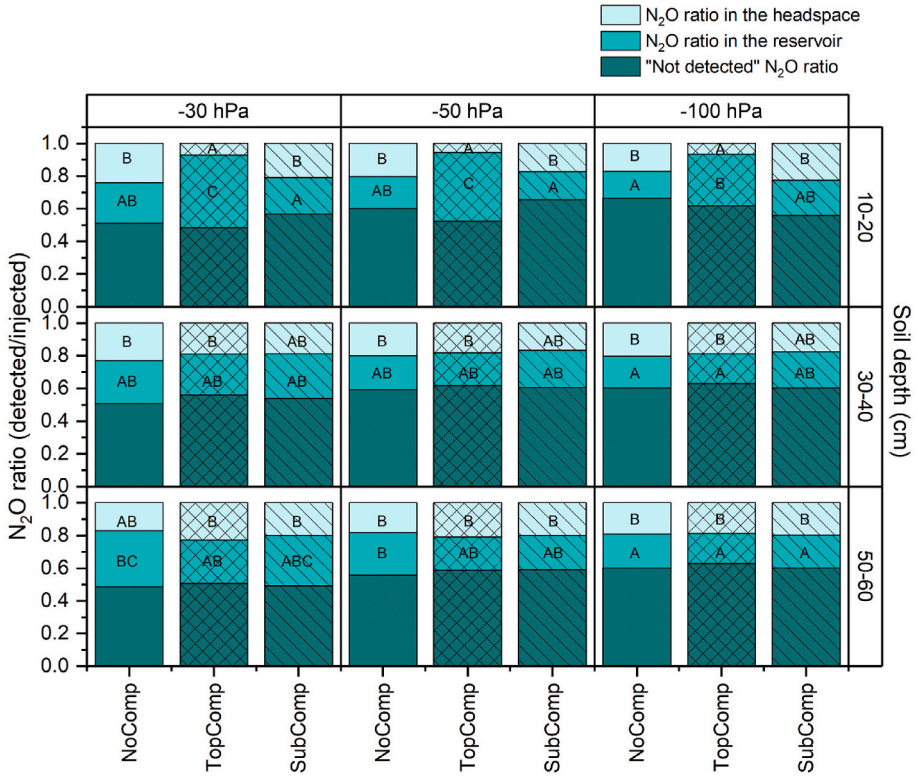

Fig. 3. The nitrous oxide (N_2O) recovery in both the headspace and the reservoir, relative to the injected N_2O concentration,30 h after the initial N_2O injection. Additionally, the corresponding "not detected" N_2O was estimated. NoComp is soil without compaction treatment, TopComp is soil with topsoil compaction treatment, and SubComp is soil with subsoil compaction treatment. Uppercase letters show the treatment × depth interaction within each soil water matric potential, at a 5% significance level.

Table 5
The ratio of nitrous oxide concentration, [N_2O], detected in the headspace, reservoir, entrapped in soil air, dissolved in soil water and the "not detected" fraction related to the initial injected [N_2O], when the soil samples were at −100 h Pa of matric potential. The "not detected" or not recovered fraction of the injected N_2O was assumed to have been transformed to N_2.

Depth (cm)	Treatment	N_2O Headspace /Injected	N_2O Reservoir /Injected	N_2O Entrapped in air-soil /Injected	N_2O Dissolved in soil water /Injected	N_2O not detected (assumed as N_2)/N_2O Injected
10–20	NoComp	0.17 ± 0.03 ABC	0.16 ± 0.03 a	0.16 ± 0.04	0.10 ± 0.02	0.41 ± 0.08
	TopComp	0.07 ± 0.03 A	0.32 ± 0.04 b	0.19 ± 0.04	0.11 ± 0.02	0.31 ± 0.08
	SubComp	0.23 ± 0.003 C	0.22 ± 0.004 ab	0.18 ± 0.04	0.11 ± 0.02	0.27 ± 0.08
30–40	NoComp	0.20 ± 0.01 BCE	0.20 ± 0.01 a	0.18 ± 0.04	0.11 ± 0.02	0.31 ± 0.08
	TopComp	0.19 ± 0.02 ABC	0.18 ± 0.02 a	0.16 ± 0.05	0.09 ± 0.03	0.38 ± 0.09
	SubComp	0.18 ± 0.02 ABC	0.22 ± 0.02 a	0.16 ± 0.04	0.09 ± 0.02	0.35 ± 0.08
50–60	NoComp	0.19 ± 0.02 ABC	0.21 ± 0.01 a	0.23 ± 0.04	0.14 ± 0.02	0.23 ± 0.08
	TopComp	0.19 ± 0.01 B	0.18 ± 0.01 a	0.30 ± 0.05	0.18 ± 0.03	0.15 ± 0.09
	SubComp	0.20 ± 0.01 B	0.20 ± 0.01 a	0.35 ± 0.06	0.21 ± 0.04	0.04 ± 0.11
P-value	*Treatment*	0.024	0.593	0.825	0.825	0.609
	Depth	*0.003*	*0.083*	*0.009*	*0.009*	*0.020*
	Treat × Depth	*<0.001*	*0.011*	*0.628*	*0.628*	*0.635*

NoComp is soil without compaction treatment, TopComp is soil with topsoil compaction treatment, and SubComp is soil with subsoil compaction treatment. Values are means with standard error (n = 4). *Treat × Depth* is the interaction of treatment and depth. Values in a column followed by a different lowercase letter significantly differ across treatments within the same depth, and uppercase letters show differences across treatments and depth, at a 5% significance level.

Table 6
Hot-water extractable organic carbon (HWEC), ammonium (NH_4–N), nitrate (NO_3–N), HWEC:NO_3, *nosZ* gene, pH and electrical conductivity (EC) of the soil samples after the injection of nitrous oxide when the soil samples were at −100hPa of soil water matric potential.

Depth (cm)	Treatment	HWEC (μg C g^{-1} soil)	NH_4–N (μg g^{-1} soil)	NO_3–N (μg g^{-1} soil)	HWEC:NO_3	*nosZ* gene 10^6 copies g dry $soil^{-1}$	pH	EC (μS cm^{-1})
10–20	NoComp	410 ± 16 ABC	0.45 ± 0.09 a	2.47 ± 0.79 BCE	275 ± 61 AB	1.28 ± 0.53 AB	7.96 ± 0.05	144 ± 7
	TopComp	491 ± 29 C	0.70 ± 0.15 a	1.09 ± 0.35 AB	677 ± 183 ABC	2.62 ± 1.35 BCE	7.99 ± 0.05	175 ± 21
	SubComp	528 ± 33 C	0.80 ± 0.11 a	5.62 ± 1.80 C	107 ± 16 A	11.79 ± 3.02 D	7.89 ± 0.05	179 ± 13
30–40	NoComp	379 ± 10 A	0.16 ± 0.11 a	0.63 ± 0.20 AB	690 ± 117 BCE	1.85 ± 0.34 B	7.99 ± 0.05	190 ± 44
	TopComp	354 ± 6 A	0.18 ± 0.03 a	0.87 ± 0.32 AB	473 ± 110 ABC	1.53 ± 0.57 AB	8.08 ± 0.06	146 ± 8
	SubComp	457 ± 19 BCE	0.33 ± 0.04 b	1.0 ± 0.32 AB	476 ± 41 BCE	5.23 ± 0.61 CD	7.98 ± 0.05	155 ± 9
50–60	NoComp	373 ± 16 AB	0.08 ± 0.02 a	0.27 ± 0.08 A	1150 ± 195 C	0.27 ± 0.12 A	7.99 ± 0.05	198 ± 40
	TopComp	362 ± 4 A	0.10 ± 0.05 a	0.73 ± 0.27 AB	646 ± 153 ABC	1.60 ± 0.80ABC	8.09 ± 0.06	146 ± 3
	SubComp	461 ± 48 ABC	0.20 ± 0.05 a	0.78 ± 0.25 AB	769 ± 205 ABC	2.77 ± 0.41 B	8.02 ± 0.05	142 ± 3
P-value	*Treatment*	*<0.001*	*<0.001*	*0.007*	*0.001*	*<0.001*	*0.179*	*0.243*
	Depth	*<0.001*	*<0.001*	*<0.001*	*<0.001*	*<0.001*	*0.109*	*0.055*
	Treat × Depth	*0.049*	*0.5643*	*0.039*	*0.034*	*0.023*	*0.874*	*0.115*

NoComp is soil without compaction treatment, TopComp is soil with topsoil compaction treatment, and SubComp is soil with subsoil compaction treatment. *Treat × Depth* is the interaction of treatment and depth. Values are means with standard error (n = 4). Values in a column followed by a different lowercase letter significantly differ across treatments within the same depth, and uppercase letters show differences across treatments and depth, at a 5% significance level.

$$log_{10}N_2O\_diffussionRatio = 1.1445\ log_{10}\ LargestMacroporeRatio - 0.6402 \quad (2)$$

To further assess the hierarchical structure of the best explanatory variables of N_2O diffusion ratio levels, a classification tree was generated using the selected data set at −100 h Pa, with satisfactory statistical performance (pruning confidence factor = 0.25, correctly classified instances = 68%, Kappa statistic = 0.43, and a root mean squared error = 0.43) (Fig. 5). The algorithm generated a tree that selected k_a as a splitting variable at the tree's root node. A low level of N_2O diffusion was classified when k_a was ≤0.001 μm^2, but when k_a was above this threshold, four decision nodes defined a sub-tree with μCT-derived total branch length, μCT-derived connected macropore ratio, D_s/D_o and μCT-derived largest macropore ratio as classificatory variables. Hence, a high degree of functional pore space for N_2O diffusion was classified for samples with a large network volume of well-connected branching macropores.

4. Discussion

4.1. Treatment, depth and matric potential effects on soil pore network

As expected, topsoil compaction decreased total porosity as both ρ_b and degree of compactness increased. The degree of compactness, in all cases, was greater than the optimal threshold of 87% reported for spring barley as a reference crop (Håkansson and Lipiec, 2000), which indicates a general poor structural arrangement, as described below.

For the TopComp treatment, at 10–20 cm, the greater ρ_b increased soil water retention (increased WFPS) while reducing ε_a and d_{eff} across matric potentials. The μCT-derived parameters also showed that macropore volume and connectivity were affected negatively by the TopComp treatment at 10–20 cm. These changes affected gas flow, and thus decreased convection (k_a and PO1) and diffusion rates (D_s/D_o) across matric potentials to levels associated with impermeable soil (Ball et al., 1988) and anaerobic conditions (Stepniewski, 1980), respectively.

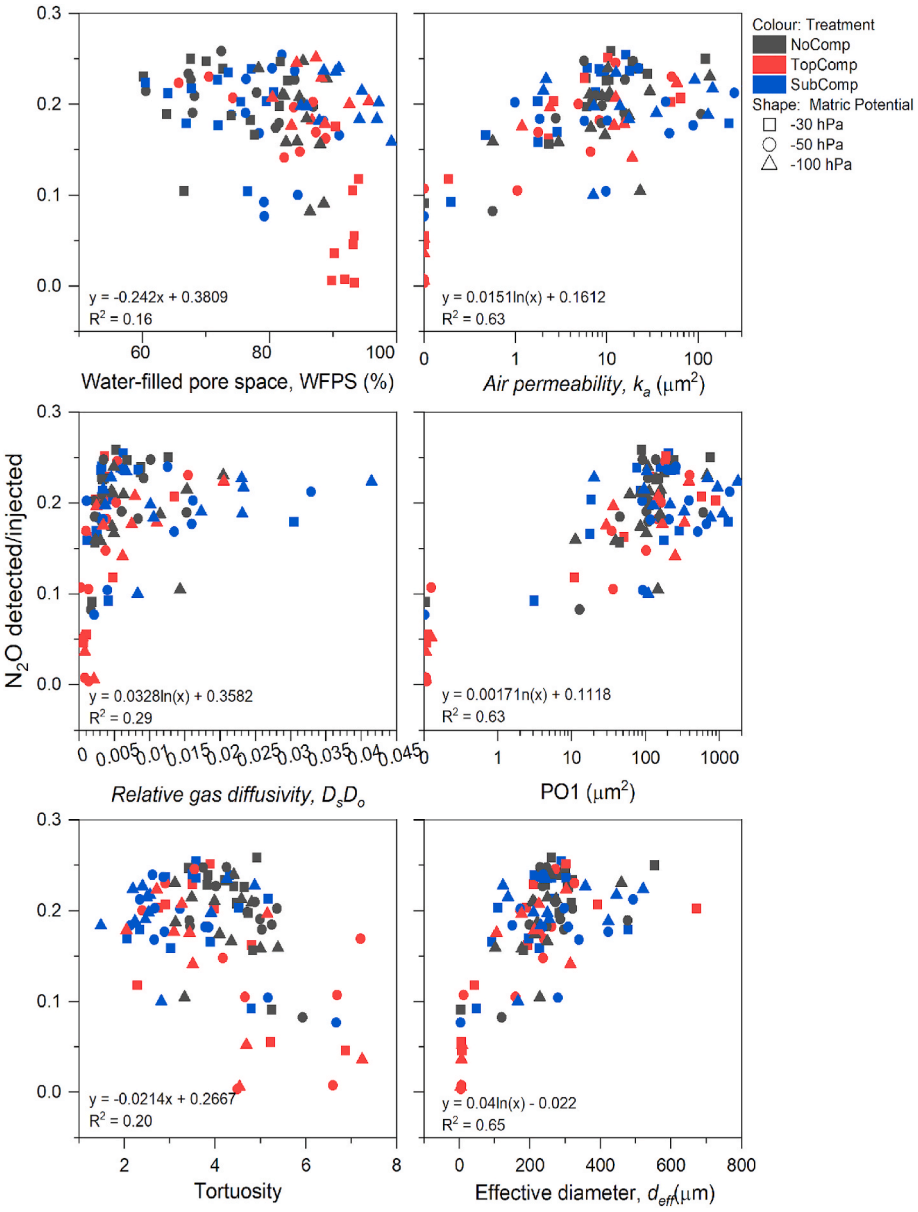

Fig. 4. Nitrous oxide (N_2O) recovery in the headspace relative to the injected N_2O concentration as a function of soil pore characteristics. NoComp is soil without compaction treatment, TopComp is soil with topsoil compaction treatment, and SubComp is soil with subsoil compaction treatment. Data points represent the values at different treatments, soil water matric potentials and soil depths.

Limited soil pore functionality was also observed at increasing soil depth in all treatments, for instance for 50–60 cm depth where soil compaction was not induced, the soils had also poor macroporosity, low gas transport, and oxygen deficiency, as indicated by values of $\varepsilon_a \leq 10\%$ (Grable and Siemer, 1968), $k_a \leq 20$ μm^2 (Fish and Koppi, 1994), and $D_s/D_o \leq 0.005$ (Stepniewski, 1980), respectively. These findings align with prior studies that have identified pore functionality constraints on gas transport in the silty soils of the Veneto low plain region, irrespective of agronomic management (i.e., no-tillage and conventional tillage) (Piccoli et al., 2017). Furthermore, it is acknowledged that roots might impact soil porosity depending on plant species, degree of soil compaction, and duration of root growth (Bodner et al., 2013; Perkons et al., 2014); however, cereal roots are expected to minimally impact pore functionality in compacted layers (Pulido-Moncada et al., 2021; Wahlström et al., 2021).

When examining the Spearman correlations between CT-derived parameters and measured gas transport parameters across depths (Supplementary Table C), as expected, a pore network with decreasing volume, lower connected macropore ratio (decreased branching), greater isolated pore ratio (increased Euler density), and greater solid-to-pore distance contributed to the observed decrease in gas transport properties such as k_a and D_s/D_o ($r = 0.69$ to 0.77, $P < 0.01$).

The observed restricted pore functionality and morphology indicate that in the studied soil, both the compaction-induced topsoil and non-compacted poor structure of the subsoil layers, could support anaerobic biological processes at water contents $\geq$ -100 hPa, with WFPS ranging from 82 to 96%. Other studies have shown physical constraints for respiration favouring denitrification in both topsoil and subsoil, especially following N application and with varying water contents (Schlüter et al., 2019; Rousset et al., 2020; Yang et al., 2022).

4.2. Soil pore network effects on nitrous oxide

In this short-term experiment, soil structural status significantly impacted N_2O diffusion within the soil layers. Soil compaction has previously been predicted to slow down N_2O transport through the soil

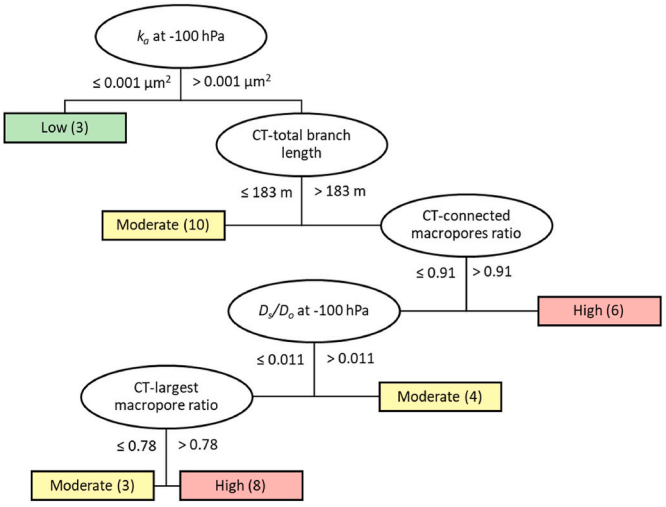

Fig. 5. The classification tree predicts the classification levels of the nitrous oxide (N_2O) diffusion ratio (N_2O detected in the headspace to the N_2O injected into the reservoir) of a silt loam soil under different soil compaction degrees. The dataset used is when the soil samples were at −100 h Pa. The pruning confidence factor was 0.25 and the total number of instances = 34. The trees generated had Correctly Classified Instances = 68%, Kappa statistic = 0.43, and Root Mean Squared Error = 0.43. Ovals are the discriminating variables and squares are the classification levels. Classificatory variables were log-transformed. k_a is air permeability, CT refers to X-ray Computed Tomography-derived parameters and D_s/D_o is relative gas diffusivity. The level of N_2O diffusion ratio was defined as "low" for ratios lower than the 0.25 percentile and "high" for values larger than the 0.75 percentile of the dataset, or else, values were classified as "moderate".

(Petersen and Abrahamsen, 2021). In the present study, the induced compaction at 10–20 cm (TopComp) favoured an earlier steady state (Fig. 2), with low N_2O concentration in the headspace when compared to the other treatments across matric potentials. Other studies have shown that diffusion time of N_2O varies due to interacting factors such as gas concentration, pathway length and tortuosity, soil type and water content (Dong et al., 2020b; Hung and Whalen, 2020).

Fig. 4 showed that on the studied soil active soil pores provided N_2O diffusive pathways even in the soil layers with $\rho_b > 1.5$ Mg m^{-3}, WFPS >90%, $k_a < 20$ µm^2, and $D_s/D_o < 0.005$. In contrast, in an earlier study by Klefoth et al. (2014) the recovery rate of injected N_2O–^{15}N was nil at 90% of WFPS and $D_s/D_o < 0.005$ for repacked silty loam soil cores, with ρ_b in the range 0.94–1.07 Mg m^{-3}. In our study, the fact that for the 10–20 cm soil layer the induced compaction (TopComp) did not completely prevent N_2O diffusion, maybe explained by the remaining presence of some conductive pores. Deformation of soil structure by compaction leads to a reduction of pore branching, promoting the dominance of vertically oriented (tube-like) pores (Dörner and Horn, 2009) with reduced diameter (Schäffer et al., 2008). Some of these altered pores may persist as active pathways (Lamandé et al., 2021).

Pore functionality also explained variation in N_2O diffusion ratio across soil depths. In the TopComp treatment, despite similar ρ_b, degree of compactness, ε_a and WFPS between the compacted topsoil for 10–20 cm and the 50–60 cm soil layer, the latter exhibited a less restrictive diffusive pathway (more connected macropores with larger d_{eff} and higher k_a and D_s/D_o), resulting in a 2.7-fold increase in N_2O diffusion ratio. For the SubComp, N_2O diffusion ratio decreased with depth in correspondence with decreasing pore transport functionality, except for D_s/D_o. Conversely, in the non-induced-compaction treatment (NoComp), the N_2O diffusion ratio did not vary with depth, despite decreasing conditions for gas transport with depth as indicated by D_s/D_o and WFPS, but not pore morphology and air permeability.

In a study by Button et al. (2023), on an uncompacted sandy clay loam soil, there was no significant difference in neither the N_2O emissions rates nor the calculated D_s/D_o with depth (0–10 cm and 50–60 cm), despite differences in ρ_b (1.11 and 1.26 Mg m^{-3}, respectively). In other studies net production rates of N_2O have been observed to differ with depth (e.g.: Shcherbak and Robertson, 2019). Differences in production and emission rates of N_2O within different layers of the soil profile, if assumed to be only physically controlled, are likely dependent on the soil structural arrangement and its related pore network functionality factors. Within an agricultural soil profile, pore arrangements are expected to differ between topsoil and subsoil, with topsoil pore network resembling a sponge-like structure, while vertical tube-like pores dominate the pore system of subsoil layer (Lamandé et al., 2021). In our study, which focused solely on N_2O diffusion within subsoil layers, it is speculated that when similar diffusion capacities are observed across depths, it may indicate preferential flow pathways in the subsoil. These pathways could emulate the diffusive capacity of sponge-like pore system in non-compacted topsoils.

On the other hand, decreasing soil matric potential (soil drainage) increases the gas diffusion coefficient (Moldrup et al., 2000) and can result in entrapped N_2O being released (Rabot et al., 2015; Balaine et al., 2016). Other studies using X-ray CT images have highlighted that this enhanced gas diffusion is mainly related to the opening of connected pores (Rohe et al., 2021; Dorau et al., 2022). In our study, the morphology of the macropores that opened with changes in matric potential was not assessed, as µCT scanning was only performed when the soil was at −100 h Pa. However, the fact that N_2O diffusion ratios did not change significantly with decreasing water content indicates that the opening of pores from −30 to −100 h Pa (i.e., >100 to 30 µm pore diameter) – in this case – had limited contribution to the connected air-filled pore volume and gas transport. In alignment with this, treatment effects on d_{eff} did not vary across matric potentials.

At −100 h Pa, the entrapment of N_2O in both air-filled pore space and dissolved in water was favoured by increases in ρ_b, degree of compactness, WFPS and CT-derived Euler density ($r = 0.396$ to 0.579, $P < 0.01$), and by decreases in CT-derived pore volume and connectivity parameters ($r = -0.460$ to -0.371, $P < 0.01$) (Supplementary Table A). Previous studies using CT analysis have shown that pore connectivity and D_s/D_o are important factors in determining the volume of entrapped N_2O (Rabot et al., 2015; Rohe et al., 2021), and also its subsequent release as the water content decreases (Dorau et al., 2022). The redistribution of soil water within the pore network has also been referred to as influencing the opening or blockage of pores at different moments (Borges et al., 2019), which is likely to alter the N_2O dynamics.

The entrapment of N_2O in air-soil pores or water slows its diffusion and increases the likelihood of total denitrification (Clough et al., 2006; Wen et al., 2016). Nevertheless, it is speculated that the greater risk of anoxic conditions in the TopComp at 10–20 cm did not cause a greater apparent N_2O reduction to N_2, as no significant differences were found for estimated N_2 ratio (not recovered N_2O/N_2O injected) across treatments and depths (Table 5).

Higher copy numbers of *nosZ* observed in the SubComp treatment suggest that subsoil compaction enhanced denitrification during N_2O transport towards the soil surface. While speculative, such a partial reduction of N_2O during diffusive transport is consistent with previous observations by Clough et al. (1998) and (2006). How ever, the copy numbers of *nosZ* did not correlate with the estimated N_2 ratio (Supplementary Table A). In a previous study in the same soil, the copy numbers of *nosZ* were similar to our results (10^6-10^7) but decreased with depth under a high fertiliser dose and shallow water table (120 cm) conditions (Cocco et al., 2018). Additionally, the work by Longepierre et al. (2022) on a fertilised sandy loam soil, showed that *nosZ* gene abundance did not significantly change under compaction across different moisture levels and crops. However, gene abundance does not necessarily link to process rates, as evidenced by Button et al. (2023) who found larger N_2O reduction in the subsoil (50–60 cm) despite lower *nosZ* gene copies in a sandy clay loam, and by Jerray et al. (2024), on a loamy soil under different cropping systems, who observed N_2O emissions depended on

denitrifier activity and environmental factors rather than denitrifier gene abundances.

The nature of denitrification involves many different factors, making it difficult to link compaction, gene abundance, substrate concentrations and N_2O diffusion/reduction ratio (Longepierre et al., 2022). Nonetheless, our results showed that for the different soil depths conditions were suitable for increasing denitrifier activity and the reduction of N_2O to N_2, specifically alkaline pH (Yamulki et al., 1997), high HWEC and low total N (Wang et al., 2021), high HWEC/NO_3 (Benckiser et al., 2015; Hung and Whalen, 2020), and high WFPS (68–93%) (Parton et al., 2001). Noticeably, HWEC was similarly distributed with depth, possibly by downward transport with percolating water, potentially supporting a homogeneous abundance of *nosZ* copies with depth (Wolf et al., 2022). High dissolved organic carbon/NO_3 ratio under anaerobic denitrifying conditions enable denitrifying organisms to use N_2O as the electron acceptor for denitrification to N_2 (Benckiser et al., 2015). In our analysis, *nosZ* gene copies showed significant positive correlation with CO_2 (Supplementary Table A), which is in line with the occurrence of the denitrification metabolism. Also, there were significant correlations of *nosZ* gene copies with HWEC and NH_4–N, consistent with denitrifiers' heterotrophic nature. Nitrate (NO_3–N) was not significantly correlated with *nosZ*. Nevertheless, higher NO_3–N in the SubComp layer aligned with higher *nosZ* copies especially at 10–20 cm depth (Table 6). As regards possible baseline abundance of the *nosZ*-bearing bacterial guild, it can be considered that where higher copy numbers of the gene are detected, this is to be considered the result of population growth having occurred upon the experimentally introduced conditions, linked to specific variables in each of the examined soil layers.

4.3. Soil-structural related factors that interact and drive the N_2O diffusion

Other studies have shown by single correlations that diffusional constraints on N_2O emissions from soils can be explained better by D_s/D_o than WFPS in soils varying in bulk density, matric potential, among others (e.g.: Petersen et al., 2008; Harrison-Kirk et al., 2015; Balaine et al., 2016; Rousset et al., 2020).

In the literature, it is also recognised that macropore volume is a sensitive indicator for dynamic structural changes related to management practices (e.g.: Pagliai et al., 2004), but its contribution to fluid transport relies on the macropore architecture (Katuwal et al., 2015; Paradelo et al., 2016; Kim et al., 2022). For example, Rabot et al. (2015) found N_2O emissions to be correlated with CT-derived connected air-filled pore volume. Rohe et al. (2021), using partial least squares regression, showed high explanatory power of CT-derived connected air-filled pore volume and CO_2 to predict N_2O emissions. Similarly, studies by Ortega-Ramírez et al. (2023) and Kravchenko et al. (2018) showed, that the proximity of particulate organic matter to air-filled pores (Euclidean distance in μCT images) was a good indicator of N_2O emissions from particulate organic matter hotspots.

However, single associations alone cannot explain the complex nature of N_2O fate, which calls for integrated approaches. Although our study used limited data, multivariate decision tree analyses were used to examine drivers influencing the upward diffusion of N_2O within soil layers, the results suggested that the N_2O diffusion ratio in the studied soil layers could be predicted based on the WFPS and k_a (Equation (1)), but when considering pore morphology characteristics, largest-macropore ratio (CT-derived pore connectivity parameter) is a better predictor variable (Equation (2)). Additionally, if N_2O diffusion ratios are classified by levels (low, moderate and high), then our data total variance could be explained by sequence thresholds of k_a, connectivity of pores (CT-derived) and D_s/D_o.

With a focus on topsoil conditions, the study by Chalco Vera et al. (2020) is an example of the use of regression tree analysis to predict N_2O and CO_2 fluxes integrating variables such as gravimetric soil moisture, soil inorganic nitrogen, ρ_b, total soil porosity and WFPS. The study suggested effective mitigating agricultural practices based on determined threshold values. Another study using path analysis suggested that soil organic carbon quality, soil moisture and total porosity control field N_2O fluxes on the studied conditions (Jerray et al., 2024).

In comparison, our study introduces the integration of soil chemical and biological parameters, laboratory-measured pore functional parameters and CT-derived pore architecture characteristics for algorithmic selection of key explanatory variables and sequences of threshold values. Our findings highlight the key role of pore connectivity characteristics and gas convection (k_a) and diffusion rates (D_s/D_o) in the regulation of N_2O fate within soil layers with varying degrees of compactness (Fig. 5). While our study simulated N_2O transport conditions within soil layers, it is important to note that in field conditions, these dynamics could also impact the diffusion of oxygen and alter the balance between aerobic and anaerobic decomposition of organic matter, thus influencing the overall net production of nitrous oxide.

Importantly, as summarised by Kravchenko and Guber (2021), interactions between management-related factors and soil structure-related factors, such as pore characteristics, are dynamic and cannot be set to an absolute value. Therefore, the complexity of factors influencing the fate of N_2O has to be assessed at different scales and scenarios. In the present study, the models were developed to describe the limited data set under site-specific conditions, but not to be used as predicting functions.

5. Conclusion

The study showed that soil compaction negatively affected N_2O diffusion, yet diffusion was still possible under restrictive conductive conditions. Estimated N_2O fractions entrapped in the air-filled pore space and dissolved in water appeared unaffected by the contrasting soil structural status across depths. The connectivity of pores (CT-derived parameters) was identified as the best explanatory variable of the N_2O diffusion ratio within the studied soil layers. This research supports the use of multivariate analysis approaches to identify the main driving factors of N_2O diffusion, along with their thresholds. These factors should be determined through a combination of soil chemical and biological parameters, pore functionality parameters and CT-derived pores morphology parameters evaluated across contrasting conditions. Our finding underscores the complex interplay of factors governing N_2O fate under compacted soils and offers insights for understanding how subsoil N_2O moves towards near-surface soil layers. The complexity of N_2O fate in the soil profile, from its production to eventual release into the atmosphere, remains a subject of ongoing research, particularly under varying soil management practices, soil types, and climate conditions.

CRediT authorship contribution statement

Mansonia Pulido-Moncada: Writing – review & editing, Writing – original draft, Visualization, Methodology, Investigation, Formal analysis, Conceptualization. **Søren O. Petersen:** Writing – review & editing, Conceptualization. **Timothy J. Clough:** Writing – review & editing, Conceptualization. **Lars J. Munkholm:** Writing – review & editing. **Andrea Squartini:** Writing – review & editing. **Matteo Longo:** Writing – review & editing. **Nicola Dal Ferro:** Writing – review & editing. **Francesco Morari:** Writing – review & editing, Funding acquisition.

Declaration of competing interest

The authors declare the following financial interests/personal relationships which may be considered as potential competing interests:

Francesco Morari reports financial support was provided by Rural Development Programme for the Veneto Region. If there are other authors, they declare that they have no known competing financial interests or personal relationships that could have appeared to influence the work reported in this paper.

Data availability

The authors do not have permission to share data.

Acknowledgements

The authors thank Carlo Camarotto, Riccardo Polese and farm staff from the Lucio Toniolo Experimental Farm of the University of Padua for their help during soil sampling and analysis. The authors also thank Massimo Dalla Benetta at the Department of Management and Engineering, University of Padua, for the technical support in CT scanning the soil cores, as well as Claudia Chiodi for her help with the *nosZ* gene quantification and Piergiorgio Stevanato for making the instrumental PCR facility available at University of Padua. The assistance of the technicians from the Agroecology Department at Aarhus University during the experimental activity and analysis is also acknowledged. Acknowledge is extended to Khagendra Raj Baral for initial discussion of experimental setup. This work was supported by Rural Development Programme for the Veneto Region PSR2021–2027.

Appendix A. Supplementary data

Supplementary data to this article can be found online at https://doi.org/10.1016/j.soilbio.2024.109536.

References

Balaine, N., Clough, T.J., Beare, M.H., Thomas, S.M., Meenken, E.D., 2016. Soil gas diffusivity controls N_2O and N_2 emissions and their ratio. Soil Science Society of America Journal 80, 529–540.
Balaine, N., Clough, T.J., Beare, M.H., Thomas, S.M., Meenken, E.D., Ross, J.G., 2013. Changes in relative gas diffusivity explain soil nitrous oxide flux dynamics. Soil Science Society of America Journal 77, 1496–1505.
Ball, B., 1981. Modelling of soil pores as tubes using gas permeabilities, gas diffusivities and water release. Journal of Soil Science 32, 465–481.
Ball, B., 2013. Soil structure and greenhouse gas emissions: a synthesis of 20 years of experimentation. European Journal of Soil Science 64, 357–373.
Ball, B., O'sullivan, M., Hunter, R., 1988. Gas diffusion, fluid flow and derived pore continuity indices in relation to vehicle traffic and tillage. Journal of Soil Science 39, 327–339.
Benckiser, G., Schartel, T., Weiske, A., 2015. Control of NO_3− and N_2O emissions in agroecosystems: a review. Agronomy for Sustainable Development 35, 1059–1074.
Bodner, G., Leitner, D., Nakhforoosh, A., Sobotik, M., Moder, K., Kaul, H.-P., 2013. A statistical approach to root system classification. Frontiers in Plant Science 4, 292.
Borges, J.A., Pires, L.F., Cassaro, F.A., Auler, A.C., Rosa, J.A., Heck, R.J., Roque, W.L., 2019. X-ray computed tomography for assessing the effect of tillage systems on topsoil morphological attributes. Soil and Tillage Research 189, 25–35.
Bremner, J.M., 1997. Sources of nitrous oxide in soils. Nutrient Cycling in Agroecosystems 49, 7–16.
Buades, A., Coll, B., Morel, J.-M., 2011. Non-local means denoising. Image Processing On Line 1, 208–212.
Bussell, J., Crotty, F., Stoate, C., 2021. Comparison of compaction Alleviation methods on soil health and greenhouse gas emissions. Land 10, 1397.
Button, E.S., Marsden, K.A., Nightingale, P.D., Dixon, E.R., Chadwick, D.R., Jones, D.L., Cárdenas, L.M., 2023. Separating N_2O production and consumption in intact agricultural soil cores at different moisture contents and depths. European Journal of Soil Science 74, 1–16.
Chalco Vera, J., Curti, R.N., Acreche, M.M., 2020. Integrating critical values of soil drivers for mitigating GHGs: an assessment in a sugarcane cropping system. Sci Total Environ 704, 135420.
Chamindu Deepagoda, T.K.K., Clough, T.J., Thomas, S.M., Balaine, N., Elberling, B., 2019a. Density effects on soil-water characteristics, soil-gas diffusivity, and emissions of N_2O and N_2 from a Re-packed pasture soil. Soil Science Society of America Journal 83, 118–125.
Chamindu Deepagoda, T.K.K., Jayarathne, J.R.R.N., Clough, T.J., Thomas, S., Elberling, B., 2019b. Soil-gas diffusivity and soil-moisture effects on N_2O emissions from intact pasture soils. Soil Science Society of America Journal 83, 1032–1043.
Chataut, G., Bhatta, B., Joshi, D., Subedi, K., Kafle, K., 2023. Greenhouse gases emission from agricultural soil: a review. Journal of Agriculture and Food Research 11, 100533.
Clough, T., Jarvis, S., Dixon, E., Stevens, R., Laughlin, R., Hatch, D., 1998. Carbon induced subsoil denitrification of ^{15}N-labelled nitrate in 1 m deep soil columns. Soil Biology and Biochemistry 31, 31–41.
Clough, T.J., Kelliher, F.M., Wang, Y.P., Sherlock, R.R., 2006. Diffusion of ^{15}N-labelled N_2O into soil columns: a promising method to examine the fate of N_2O in subsoils. Soil Biology and Biochemistry 38, 1462–1468.
Clough, T.J., Sherlock, R.R., Rolston, D.E., 2005. A review of the Movement and fate of N_2O in the subsoil. Nutrient Cycling in Agroecosystems 72, 3–11.
Cocco, E., Bertora, C., Squartini, A., Delle Vedove, G., Berti, A., Grignani, C., Lazzaro, B., Morari, F., 2018. How shallow water table conditions affect N_2O emissions and associated microbial abundances under different nitrogen fertilisations. Agriculture, Ecosystems & Environment 261, 1–11.
Davidson, E., Firestone, M., 1988. Measurement of nitrous oxide dissolved in soil solution. Soil Science Society of America Journal 52, 1201–1203.
Dong, S., Li, Y., Ganjurjav, H., Gao, Q., Gao, X., Zhang, J., Yan, Y., Zhang, Y., Liu, S., Hu, G., 2020a. Grazing promoted soil microbial functional genes for regulating C and N cycling in alpine meadow of the Qinghai-Tibetan Plateau. Agriculture, Ecosystems & Environment 303, 107111.
Dong, W., Walkiewicz, A., Bieganowski, A., Oenema, O., Nosalewicz, M., He, C., Zhang, Y., Hu, C., 2020b. Biochar promotes the reduction of N_2O to N_2 and concurrently suppresses the production of N_2O in calcareous soil. Geoderma 362, 114091.
Dorau, K., Uteau, D., Hövels, M.P., Peth, S., Mansfeldt, T., 2022. Soil aeration and redox potential as function of pore connectivity unravelled by X-ray microtomography imaging. European Journal of Soil Science 73, e13165.
Dörner, J., Horn, R., 2009. Direction-dependent behaviour of hydraulic and mechanical properties in structured soils under conventional and conservation tillage. Soil and Tillage Research 102, 225–232.
Doube, M., 2021. Multithreaded two-pass connected components labelling and particle analysis in ImageJ. Royal Society Open Science 8, 201784.
Fish, A., Koppi, A., 1994. The use of a simple field air permeameter as a rapid indicator of functional soil pore space. Geoderma 63, 255–264.
Ghani, A., Dexter, M., Perrott, K., 2003. Hot-water extractable carbon in soils: a sensitive measurement for determining impacts of fertilisation, grazing and cultivation. Soil Biology and Biochemistry 35, 1231–1243.
Gil-Loaiza, J., Roscioli, J.R., Shorter, J.H., Volkmann, T.H.M., Ng, W.-R., Krechmer, J.E., Meredith, L.K., 2022. Versatile soil gas concentration and isotope monitoring: optimization and integration of novel soil gas probes with online trace gas detection. Biogeosciences 19, 165–185.
Goldberg, S.D., Gebauer, G., 2009a. Drought turns a Central European Norway spruce forest soil from an N_2O source to a transient N_2O sink. Global Change Biology 15, 850–860.
Goldberg, S.D., Gebauer, G., 2009b. N2O and NO fluxes between a Norway spruce forest soil and atmosphere as affected by prolonged summer drought. Soil Biology and Biochemistry 41, 1986–1995.
Grable, A.R., Siemer, E., 1968. Effects of bulk density, aggregate size, and soil water suction on oxygen diffusion, redox potentials, and elongation of corn roots. Soil Science Society of America Journal 32, 180–186.
Groenevelt, P., Kay, B., Grant, C., 1984. Physical assessment of a soil with respect to rooting potential. Geoderma 34, 101–114.
Håkansson, I., Lipiec, J., 2000. A review of the usefulness of relative bulk density values in studies of soil structure and compaction. Soil and Tillage Research 53, 71–85.
Hall, M., Frank, E., Holmes, G., Pfahringer, B., Reutemann, P., Witten, I.H., 2009. The WEKA data mining software: an update. ACM SIGKDD explorations newsletter 11, 10–18.
Hallin, S., Philippot, L., Löffler, F.E., Sanford, R.A., Jones, C.M., 2018. Genomics and ecology of novel N2O-reducing microorganisms. Trends in Microbiology 26, 43–55.
Harrison-Kirk, T., Thomas, S.M., Clough, T.J., Beare, M.H., van der Weerden, T.J., Meenken, E.D., 2015. Compaction influences N_2O and N_2 emissions from ^{15}N-labeled synthetic urine in wet soils during successive saturation/drainage cycles. Soil Biology and Biochemistry 88, 178–188.
Hernandez-Ramirez, G., Ruser, R., Kim, D.-G., 2021. How does soil compaction alter nitrous oxide fluxes? A meta-analysis. Soil and Tillage Research 211, 105036.
Hu, W., Drewry, J., Beare, M., Eger, A., Müller, K., 2021. Compaction induced soil structural degradation affects productivity and environmental outcomes: a review and New Zealand case study. Geoderma 395, 115035.
Hung, C.-Y., Whalen, J.K., 2020. Biophysical controls on nitrous oxide emissions following rain-induced thawing of frozen soil microcosms by simulated rainfall. Soil Biology and Biochemistry 149, 107960.
IUSS-WorkingGroup-WRB, 2015. World Reference Base for Soil Resources 2014, update 2015, International soil classification system for naming soils and creating legends for soil maps. In: Schad P, v.H.C., Micheli, E. (Eds.), World Soil Resources Reports. FAO, Rome, p. 192.
Jerray, A., Rumpel, C., Le Roux, X., Massad, R., Chabbi, A., 2024. N2O emissions from cropland and grassland management systems are determined by soil organic matter quality and soil physical parameters rather than carbon stock and denitrifier abundances. Soil Biology and Biochemistry 190, 109274.
Jones, M.W., Peters, G.P., Gasser, T., Andrew, R.M., Schwingshackl, C., Gütschow, J., Houghton, R.A., Friedlingstein, P., Pongratz, J., Le Quéré, C., 2023. National contributions to climate change due to historical emissions of carbon dioxide, methane, and nitrous oxide since 1850. Scientific Data 10, 155.
Katuwal, S., Norgaard, T., Moldrup, P., Lamandé, M., Wildenschild, D., de Jonge, L.W., 2015. Linking air and water transport in intact soils to macropore characteristics inferred from X-ray computed tomography. Geoderma 237, 9–20.
Keller, T., Håkansson, I., 2010. Estimation of reference bulk density from soil particle size distribution and soil organic matter content. Geoderma 154, 398–406.
Kim, K., Gil, J., Ostrom, N.E., Gandhi, H., Oerther, M.S., Kuzyakov, Y., Guber, A.K., Kravchenko, A.N., 2022. Soil pore architecture and rhizosphere legacy define N2O production in root detritusphere. Soil Biology and Biochemistry 166, 108565.
Klefoth, R.R., Clough, T.J., Oenema, O., Van Groenigen, J.-W., 2014. Soil bulk density and moisture content influence relative gas diffusivity and the reduction of nitrogen-^{15} nitrous oxide. Vadose Zone Journal 13.
Koestel, J., Schlüter, S., 2019. Quantification of the structure evolution in a garden soil over the course of two years. Geoderma 338, 597–609.

Kravchenko, A., Guber, A., 2021. Imaging soil structure to measure soil functions and soil health with X-ray computed micro-tomography. In: Otten, W. (Ed.), Advances in Measuring Soil Health. Burleigh Dodds Science Publishing, London, pp. 111–138.
Kravchenko, A.N., Guber, A.K., Quigley, M.Y., Koestel, J., Gandhi, H., Ostrom, N.E., 2018. X-ray computed tomography to predict soil N_2O production via bacterial denitrification and N_2O emission in contrasting bioenergy cropping systems. GCB Bioenergy 10, 894–909.
Lamandé, M., Schjønning, P., Dal Ferro, N., Morari, F., 2021. Soil pore system evaluated from gas measurements and CT images: a conceptual study using artificial, natural and 3D-printed soil cores. European Journal of Soil Science 72, 769–781.
Laudone, G.M., Matthews, G.P., Bird, N.R.A., Whalley, W.R., Cardenas, L.M., Gregory, A. S., 2011. A model to predict the effects of soil structure on denitrification and N_2O emission. Journal of Hydrology 409, 283–290.
Longepierre, M., Feola Conz, R., Barthel, M., Bru, D., Philippot, L., Six, J., Hartmann, M., 2022. Mixed effects of soil compaction on the nitrogen cycle under pea and wheat. Frontiers in Microbiology 12, 4306.
Longo, M., Jones, C.D., Izaurralde, R.C., Cabrera, M.L., Dal Ferro, N., Morari, F., 2021. Testing the EPIC Richards submodel for simulating soil water dynamics under different bottom boundary conditions. Vadose Zone Journal 20, 20142.
Lucas, M., Gil, J., Robertson, G., Ostrom, N., Kravchenko, A., 2023. Changes in soil pore structure generated by the root systems of maize, sorghum and switchgrass affect in situ N_2O emissions and bacterial denitrification. Biology and Fertility of Soils. https://doi.org/10.1007/s00374-00023-01761-00371.
Moldrup, P., Olesen, T., Schjønning, P., Yamaguchi, T., Rolston, D., 2000. Predicting the gas diffusion coefficient in undisturbed soil from soil water characteristics. Soil Science Society of America Journal 64, 94–100.
Ortega-Ramírez, P., Pot, V., Laville, P., Schlüter, S., Amor-Quiroz, D.A., Hadjar, D., Mazurier, A., Lacoste, M., Caurel, C., Pouteau, V., 2023. Pore distances of particulate organic matter predict N_2O emissions from intact soil at moist conditions. Geoderma 429, 116224.
Pagliai, M., Vignozzi, N., Pellegrini, S., 2004. Soil structure and the effect of management practices. Soil and Tillage Research 79, 131–143.
Paradelo, M., Katuwal, S., Moldrup, P., Norgaard, T., Herath, L., de Jonge, L.W., 2016. X-ray CT-derived soil characteristics explain varying air, water, and solute transport properties across a loamy field. Vadose Zone Journal 15, vzj2015, 2007.0104.
Parton, W., Holland, E., Del Grosso, S., Hartman, M., Martin, R., Mosier, A., Ojima, D., Schimel, D., 2001. Generalized model for NO_x and N_2O emissions from soils. Journal of Geophysical Research: Atmospheres 106, 17403–17419.
Perkons, U., Kautz, T., Uteau, D., Peth, S., Geier, V., Thomas, K., Holz, K.L., Athmann, M., Pude, R., Köpke, U., 2014. Root-length densities of various annual crops following crops with contrasting root systems. Soil and Tillage Research 137, 50–57.
Petersen, C.T., Abrahamsen, P., 2021. Predicting effects of soil compaction on crop yield and nitrogen dynamics. Tidsskrift for Landøkonomi 4, 293–300.
Petersen, S.O., Hoffmann, Carl C., Schäfer, C.-M., Blicher-Mathiesen, G., Elsgaard, L., Kristensen, K., Larsen, S.E., Torp, S.B., Greve, M.H., 2012. Annual emissions of CH_4 and N_2O, and ecosystem respiration, from eight organic soils in Western Denmark managed by agriculture. Biogeosciences 9, 403–422.
Petersen, S.O., Schjønning, P., Thomsen, I.K., Christensen, B.T., 2008. Nitrous oxide evolution from structurally intact soil as influenced by tillage and soil water content. Soil Biology and Biochemistry 40, 967–977.
Piccoli, I., Schjønning, P., Lamandé, M., Furlan, L., Morari, F., 2017. Challenges of conservation agriculture practices on silty soils. Effects on soil pore and gas transport characteristics in North-eastern Italy. Soil and Tillage Research 172, 12–21.
Pulido-Moncada, M., Monnereau, C., Munkholm, L.J., 2021. Root-dependent recovery of pore system functionality of compacted subsoil: a field case study with bio-subsoilers in Denmark. Soil Science Society of America Journal 85, 1566–1577.
Pulido-Moncada, M., Petersen, S.O., Munkholm, L.J., 2022. Soil compaction raises nitrous oxide emissions in managed agroecosystems. A review. Agronomy for Sustainable Development 42, 1–26.
Rabot, E., Lacoste, M., Hénault, C., Cousin, I., 2015. Using X-ray computed tomography to describe the dynamics of nitrous oxide emissions during soil drying. Vadose Zone Journal 14, 1–10.
Rohe, L., Apelt, B., Vogel, H.-J., Well, R., Wu, G.-M., Schlüter, S., 2021. Denitrification in soil as a function of oxygen availability at the microscale. Biogeosciences 18, 1185–1201.
Rösch, C., Mergel, A., Bothe, H., 2002. Biodiversity of denitrifying and dinitrogen-fixing bacteria in an acid forest soil. Applied and Environmental Microbiology 68, 3818–3829.
Roscioli, J.R., Meredith, L.K., Shorter, J.H., Gil-Loaiza, J., Volkmann, T.H.M., 2021. Soil gas probes for monitoring trace gas messengers of microbial activity. Scientific Reports 11, 8327.
Rousset, C., Clough, T.J., Grace, P.R., Rowlings, D.W., Scheer, C., 2020. Soil type, bulk density and drainage effects on relative gas diffusivity and N_2O emissions. Soil Research 58, 726–736.
Rueden, C.T., Schindelin, J., Hiner, M.C., DeZonia, B.E., Walter, A.E., Arena, E.T., Eliceiri, K.W., 2017. ImageJ2: ImageJ for the next generation of scientific image data. BMC Bioinformatics 18, 1–26.
Schäffer, B., Mueller, T., Stauber, M., Müller, R., Keller, M., Schulin, R., 2008. Soil and macro-pores under uniaxial compression. II. Morphometric analysis of macro-pore stability in undisturbed and repacked soil. Geoderma 146, 175–182.
Schjønning, P., Eden, M., Moldrup, P., de Jonge, L.W., 2013. Two-chamber, two-gas and one-chamber, one-gas methods for measuring the soil-gas diffusion coefficient: validation and inter-calibration. Soil Science Society of America Journal 77, 729–740.
Schjønning, P., Koppelgaard, M., 2017. The Forchheimer approach for soil air permeability measurement. Soil Science Society of America Journal 81, 1045–1053.
Schjønning, P., McBride, R., Keller, T., Obour, P., 2017. Predicting soil particle density from clay and soil organic matter contents. Geoderma 286, 83–87.
Schlüter, S., Vogel, H.-J., 2016. Analysis of soil structure turnover with garnet particles and X-ray microtomography. PLoS One 11, e0159948.
Schlüter, S., Zawallich, J., Vogel, H.-J., Dörsch, P., 2019. Physical constraints for respiration in microbial hotspots in soil and their importance for denitrification. Biogeosciences 16, 3665–3678.
Shcherbak, I., Robertson, G.P., 2019. Nitrous oxide (N_2O) emissions from Subsurface soils of agricultural Ecosystems. Ecosystems 22, 1650–1663.
Stepniewski, W., 1980. Oxygen-diffusion and strength as related to soil compaction. I. ODR. Polish Journal of Soil Science 13, 3–13.
Team-RDC, 2021. R: A Language and Environment for Statistical Computing. R Foundation for Statistical Computing, Vienna, Austria.
Tian, H., Xu, R., Canadell, J.G., Thompson, R.L., Winiwarter, W., Suntharalingam, P., Davidson, E.A., Ciais, P., Jackson, R.B., Janssens-Maenhout, G., 2020. A comprehensive quantification of global nitrous oxide sources and sinks. Nature 586, 248–256.
Tsai, W.-H., 1985. Moment-preserving thresholding: a new approach. Computer Vision, Graphics, and Image Processing 29, 377–393.
Wahlström, E.M., Kristensen, H.L., Thomsen, I.K., Labouriau, R., Pulido-Moncada, M., Nielsen, J.A., Munkholm, L.J., 2021. Subsoil compaction effect on spatio-temporal root growth, reuse of biopores and crop yield of spring barley. European Journal of Agronomy 123, 126225.
Wang, C., Amon, B., Schulz, K., Mehdi, B., 2021. Factors that influence nitrous oxide emissions from agricultural soils as well as their representation in simulation models: a review. Agronomy 11, 770.
Wen, Y., Chen, Z., Dannenmann, M., Carminati, A., Willibald, G., Kiese, R., Wolf, B., Veldkamp, E., Butterbach-Bahl, K., Corre, M.D., 2016. Disentangling gross N_2O production and consumption in soil. Scientific Reports 6, 36517.
Wolf, K.A., Børgesen, C.D., Plauborg, F., Petersen, S.O., 2022. Nitrous oxide and nitrate as indicators of subsoil removal of N in pig slurry applied to Luvisols in Western Denmark. Geoderma Regional 28, e00441.
Yamulki, S., Harrison, R.M., Goulding, K., Webster, C., 1997. N_2O, NO and NO_2 fluxes from a grassland: effect of soil pH. Soil Biology and Biochemistry 29, 1199–1208.
Yang, P., Reijneveld, A., Lerink, P., Qin, W., Oenema, O., 2022. Within-field spatial variations in subsoil bulk density related to crop yield and potential CO_2 and N_2O emissions. Catena 213, 106156.